Chapter 12

Perovskite as Light Harvester: Prospects, Efficiency, Pitfalls and Roadmap

Ruby Srivastava

Additional information is available at the end of the chapter

http://dx.doi.org/10.5772/65052

Abstract

In the recent years, perovskite materials have attracted great attention due to their excellent light-harvesting properties. The organic materials of these hybrid inorganic organic light harvesters are used as sensitizers and the inorganic materials have been used as light absorbers. The exceptional properties of these materials such as long diffusion length, high carrier mobility, affordable device fabrication, and adjustable adsorption range have created a new era in optoelectronic technologies. The perovskites have become promising materials due of their versatility in device architecture, flexibility in material growth, and ability to achieve the high efficiency through various processing techniques. The superior performance of silicon-based tandems by achieving efficiency more than 40% has encouraged researchers to further expand the investigations to higher levels. The quest to transit the research curiosity to the market photovoltaic technology has given a new dimension to the remarkable ascension of perovskite solar cells. This chapter introduces the experimental and theoretical aspects, the electrical and optical properties, pitfalls, and a roadmap for the future prospects of perovskite materials.

Keywords: perovskite, power conversion efficiency, energy conversion and storage, toxicity, hysteresis

1. Introduction

The fast-paced industrial development and population growth has increased the consumption of global energy to such an extent that it has become the ultimate necessity to use the renewable energy resources for long-term sustainable development. Now it has become a challenge for both scientists and technologists to generate the cost-effective and environmentally friendly renewable energy resources [1, 2].

Although solar cells based on the photovoltaic effect have attracted great attention due to the advantage of decentralization and sustainability, yet they suffer low cost effectiveness. Another emerging class of thin-film energy devices based on amorphous silicon also tried to capture the market, making headway by processing of costs per unit area [3–5]. The manufacturing of inorganic thin-films solar cells needs high-temperature and high vacuum-based techniques [6]. In addition, these techniques are limited and due to the inclusion of toxic elements, they are limited to large-scale production and wide applications [7].

In 1991, a new breakthrough emerged in the form of dye-sensitized solar cells (DSSCs) that have attracted considerable attention due to their potential application in low-cost solar energy conversion [8–16]. A high efficiency exceeding 12% was obtained by using 10 μm mesoporous TiO_2 film sensitized with a cobalt redox electrolyte and an organic dye [17]. Furthermore, solid-state DSSCs were also investigated where the liquid electrolyte was replaced by a solid hole-transporting material (HTM) [e.g., poly(3-hexylth-iophene)(P3HT),2,2′,7,7′-tetrakis-(N,N-di-p-methoxyphenyl-amine)-9,9′spirobifluorene (spiro-MeOTAD)], polyaniline, and polypyrrole [8] to increase the open circuit voltage and stability of solar cells [18–22]. However, these ss-DSSCs also suffer from faster electron recombination dynamics between electrons (TiO_2) and holes (hole transporter), which results in the low efficiency of ss-DSSCs [23]. So attempts were made to design various types of cells to increase the efficiency of solar cells [24].

This efficiency criterion was increased by the introduction of the perovskite sensitizer ABX_3 (A = CH_3NH_3, B = Pb, Sn, and X = Cl, Br, I), introduced by Prof. Grätzel and team, which has opened a new era in the field of DSSCs due to the excellent light-harvesting capabilities [24–37]. These materials are composed of earth abundant materials, inexpensive, processable at low temperatures (printing techniques), generate charges freely (after absorption) in bulk materials, which qualify them as low energy-loss charge generators and collectors [38–40]. Methylammonium lead trihalide ($CH_3NH_3PbX_3$, where X is a halogen ion such as I^-, Br^-, and Cl^-) have an optical bandgap between 2.3 and 1.6 eV depending on halide content, while formamidinum lead trihalide ($H_2NCHNH_2PbX_3$) also have a bandgap between 2.2 and 1.5 eV. The minimum bandgap is closer to optimum for a single-junction cell than methylammonium lead trihalide, which enhance to higher efficiencies [41]. The power conversion efficiency (PCE) of perovskite cells was improved from 7.2 to 15.9%, which is associated with the comparable optical absorption length and charge-carrier diffusion lengths, making this device the most outperforming relative to the other third-generation thin-film solar cell technologies. Although two different configurations using $CH_3NH_3PbI_3$ perovskite in a classical solid-state DSSC and in a thin-film planar configuration with $CH_3NH_3PbI_{3-x}Cl_x$, having efficiency exceeding 16%, have been reported [26, 42], provided few issues related to the stability and hysteresis are to be solved effectively [43].

Here, it is necessary to mention that the lack of hysteresis that was an obstacle for stable operation in perovskite was observed recently using thin films of organometallic perovskites with millimeter-scale crystalline grains with efficiencies approximately equal to 18% [44].

The three recent reports have given high hopes in the field of solar cells as EPFL scientists have developed a new hole-transporting material FDT that can reduce the cost and achieve

the power conversion efficiency of 20.2% [45]. Another study by Hong Kong University claims that they have achieved the highest efficiency of 25.5% by perovskite-silicon tandem solar cells [46]. In the meantime, it has been claimed that the efficiency of more than 30% can be achieved by tandem solar cells based on silicon and perovskites [47].

2. Structure of perovskite materials

The basic structure of perovskite consists of a 3D network corner-sharing BX_6 octahedra, where A (e.g., A = Cs, CH_3NH_3, NH_2CHNH_2) cations are located in the larger 12-fold coordinated holes between the octahedra [44]. It is composed of a metal cation (M = Sn, Pb, Ge, Cu) and its ligantanions (X = O^{2-}, Cl^-, Br^-, I^-, or S^{2-}). In the case of inorganic perovskite compounds, the structures can be distorted as a result of the cation displacements, which give rise to some useful properties of ferroelectricity and antiferroelectricity due to the stereochemically active pairs of A cations [48]. The simple cubic structure of $CH_3NH_3PbI_3$ is given in **Figure 1**.

These inorganic-organic hybrid compounds have the advantages of inorganic components that include structural order and thermal stability with interesting characteristics of organic materials such as low cost, mechanical flexibility, and functional versatility [49–53]. Numerous compounds have been reported by the covalent bonding between the inorganic and organic bonds [54]. Although the degree of interactions in organic-inorganic systems with the van der Waals interacting system is relatively small, the reason for the small van der Waals interaction is the choice of organic cations, which is limited as the restricted dimension of the cuboctahedral hole formed by the 12 nearest-neighbor X atoms. The synthesis of compounds CH_3NH_3 MX_3 with M = Sn, Pb and X= Cl, Br, and I has been successfully carried out by some groups [55–57]. These organic cations show orientational disorder at high temperature, while at lower temperature the cubic phase results in a structural phase transition as the tolerance factor is smaller than unity. Upon cooling, the structure distorts to lower its symmetry as there are many restrictions to the motion of methylammonium cations [57].

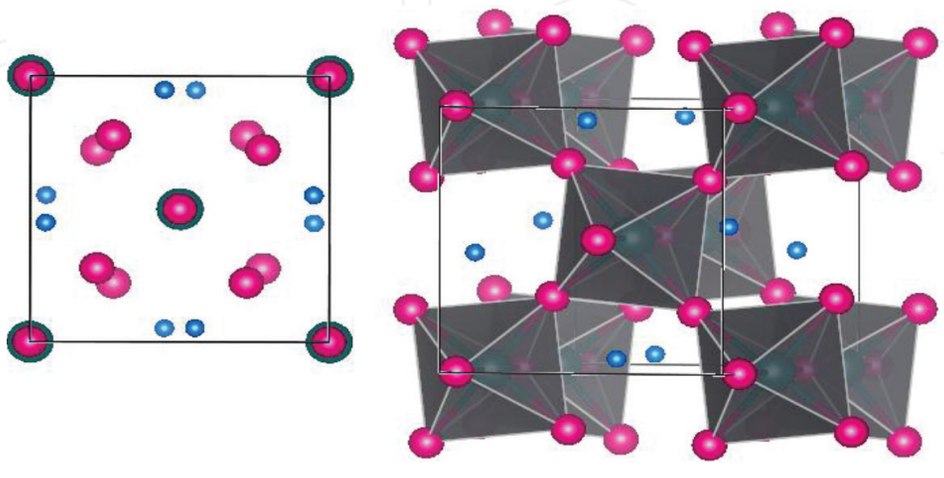

Figure 1. The crystal structure of perovskites, ABX_3, a large cation (A) at center together with metal cation (B) bonded to the surrounded halides (X). Color code: A (CH_3NH_3),blue; B (Pb), green; and X (I), pink.

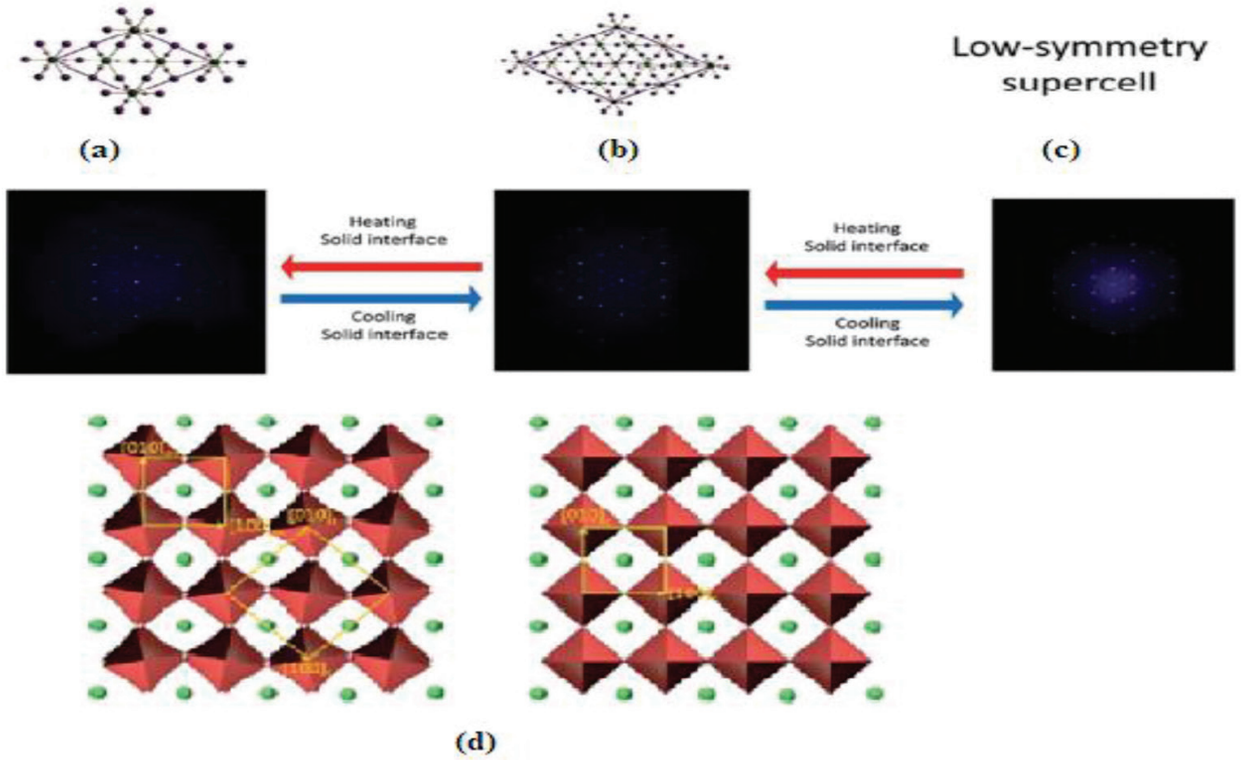

Figure 2. Graphical representation of phase transitions of MA(Pb, Sn)X_3 perovskite materials (a) α-phase, (b) β-phase, (c) γ-phase. Precision images are taken at the [006] view. (d) The structural transformation of Br included in $MAPbI_3$. Adapted with permission from reference [37].

MA, FA, Pb, and Sn perovskite combinations to identify three distinct phase transitions that occur are classified as a high temperature α phase, an intermediate β temperature phase, and a low temperature γ phase [54]. These different phases are represented in **Figure 2**.

The perovskites were first investigated by Goldschmidt in the 1920s [58] in work related to tolerance factors. The tolerance factor, t, with respect to the ionic radius of the actual ions is given in Eq. (1), where r_A, r_B, and r_C are the ionic radius of the A, B, and C ions, respectively.

$$t = \frac{r_A + r_C}{\sqrt{2}\left(r_B + r_C\right)} \tag{1}$$

The tolerance factor of (0.9–1) is for an ideal cubic structure, for a cubic structure with the tolerance factor (0.7–0.9), the A ion is too small or the B ion is too large. This can be resulted in orthorhombic, rhombohedral, or tetragonal structure. For a large A cation, t becomes larger than one, which results in layered perovskite structures [59, 60]. The compiled results are given in **Table 1** and the different forms of perovskite material $CH_3NH_3PbI_3$ are given in **Figure 3**. The expected structure is also related to Pauling's rules (PRs) [61], given the expected coordination around a two-component radii (cation/anion) system which is summarized in **Table 2**.

The smaller tolerance factor is related to lower symmetry tetragonal or orthorhombic structures, whereas larger t ($t > 1$) could destabilize the three-dimensional (3D) B-X network.

Structure	Tolerance factor	Comment for cation/anion
Tetragonal/rhombohedral/ orthorhombic	0.7–0.9	Cation too large or anion too small
Cubic	0.9–1.0	Ideal perovskite
Layered structures	>1.0	Cation too large

Table 1. Tolerance factors for the perovskite structures

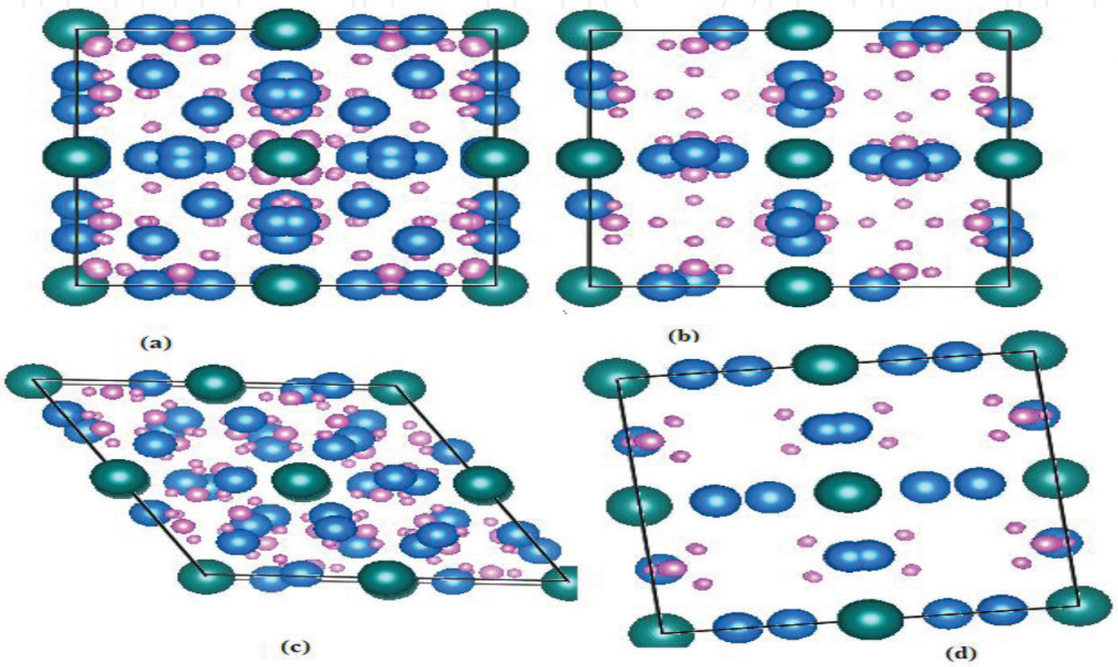

Figure 3. The crystal structure of perovskites ($CH_3NH_3PbI_3$) in different forms: (a) cubic, (b) tetragonal, (c) rhombohedral, and (d) orthorhombic. Color code: CH_3NH_3, pink; Pb, green and I, blue.

Coordination	r_c/r_a	Coordination number
0.15–0.22	Triangular	3
0.22–0.41	Tetrahedral	4
0.41–0.73	Octahedral	6
0.73–1.0	Cubic	8

Table 2. Coordination and ideal $r_c r_a$ (Pauling's rules). r_c and r_a represent the cationic and anionic radii

The other important parameter is an octahedral factor that plays an important role in these materials, and is given by,

$$\mu = R_B / R_A \tag{2}$$

where R_B is the ionic radii of the B cation and R_A is the ionic radii of A anion. If $\mu > 0.442$, the formation of halide perovskite achieves, whereas below this value BX_6 octahedron will

become unstable and a perovskite structure will not form, although these factors provide a guidelines for the formation of halide perovskite, yet they are not sufficient to predict the structural formations within the perovskite family [62].

2.1. Experimental scenario

2.1.1. Origin of perovskite

Although these materials already possessed useful physical properties, organic-like mobility, nonlinear optical properties, enhanced exciton binding energies, electroluminescence, magnetic properties, and conductivity, they have emerged as DSSCs only in 2009 [63–68]. The performance of DSSCs is assessed by three major parameters: short-circuit photocurrent (J_{SC}), open-circuit voltage (V_{OC}), and fill factor (FF), which are further used to calculate the efficiency (PCE). V_{OC} is proportional to the HOMO-LUMO energy gap and J_{SC} reflects the mobility, efficient light-harvesting, and carrier generation. These values of different device structures are presented in **Table 3**.

The first perovskite-sensitized TiO_2 solar cell gave the efficiency of 3.8 and 3.1%, respectively [13]. Later on the titania's surface and $CH_3NH_3PbI_3$-based iodide liquid electrolyte solar cell have increased the efficiency to 6.5% [25]. In 2012, the liquid electrolyte was replaced with a solid electrolyte and a PCE of 9.7% was achieved [69]. A sequential deposition method for the formation of the perovskite pigment within the porous metal oxide film was developed with a PCE of 15% in 2013 (short-circuit current density J_{SC} = 21.5 mA/cm^2, open-circuit voltage V_{OC} = 1.02 V, and fill factor FF = 0.71) [27]. An efficiency of 20% at low temperature was achieved in a processed solar cell, through the end of 2013 [70, 71]. Further, it is reported that the achieved efficiency has above 30% in 2016.

2.1.2. Photoanodes

Mesoporous metal oxide films act as a working electrode for perovskite cells. The charge extraction rates are relatively faster for the perovskite solar cells than the conventional DSSCs [39]. Again the mesoporous TiO_2 was replaced by Al_2O_3 with similar mesomorphology and it was seen that the PCE unexpectedly reached to 10.9% giving hopes for the future increase in efficiency. Furthermore, the DSSC efficiency has improved to 15.9% [27], yet there is the difficulty in pore filling because of the labyrinthine maze structure [72], which was alternatively substituted by a vertically aligned nanowire (NW) and nanotube (NT) structure. These nanotubes and nanowires can be used in pore filling due to their open porous structures. Moreover, they are reported to be better in electron transportation and recombination behavior and hole conductors presenting faster recombination than nanoparticulate films in liquid-based DSSCs [73–75].

As the absorption properties of perovskite are excellent, a possible decrease in the total surface area of the NWs/NTs compared to the nanoparticles does not stimulate the significant reduction of photocurrent. Later it was concluded that perovskite semiconductors in their simple architecture can exhibit sufficiently good ambipolar charge transport and the principal roles of photovoltaic operation, including charge generation, light absorption, and transport

Perovskite	Photo anode	HTM	J_{SC} (mA/cm)	V_{OC} (v)	FF	PCE (%)	References
$CH_3NH_3PbI_3$	mp (TiO_2)	Spiro	17.6	0.88	0.62	9.7	[69]
$CH_3NH_3PbI_3$	TiO_2 NS	Spiro	16.1	0.63	0.57	5.5	[30]
$CH_3NH_3PbI_3$	mp (TiO_2)	Spiro	18.8	0.71	0.66	8	[70]
$CH_3NH_3PbI_3$	mp (TiO_2)	Spiro	18.3	0.87	0.66	10.4	[71]
$CH_3NH_3PbI_2Cl$	mp (Al_2O_3)	Spiro	17.8	0.98	0.63	10.9	[26]
$CH_3NH_3PbI_3$	TiO_2-NWAs	Spiro	10.67	0.74	0.54	4.29	[72]
$CH_3NH_3PbI_2Br$	TiO_2-NWAs	Spiro	10.12	0.82	0.59	4.87	[72]
$CH_3NH_3PbI_3$	mp (TiO_2)	Spiro	20.0	0.99	0.73	15.0	[73]
$CH_3NH_3PbI_3$	Rutile (TiO_2)	Spiro	15.6	0.95	0.63	9.4	[74]
$CH_3NH_3PbI_3$	mp-ZrO_2	Spiro	17.3	1.07	0.59	10.8	[75]
$CH_3NH_3PbI_3$	(TiO_2)crystal	Spiro	12.86	0.79	0.70	7.29	[76]
$CH_3NH_3PbI_3$	mp (Al_2O_3)	Spiro	18.0	1.02	0.67	12.3	[37]
$CH_3NH_3PbI_3$	$CH_3NH_3PbI_3$	Spiro	21.5	1.07	0.67	15.4	[77]
$CH_3NH_3PbI_3$	mp (TiO_2)	P3HT	12.6	0.73	0.73	6.7	[42]
$CH_3NH_3PbI_3$	mp (TiO_2)	PCPDTBT	10.3	0.77	0.67	5.3	[42]
$CH_3NH_3PbI_3$	mp (TiO_2)	PCPDTBT	10.5	0.92	0.43	4.2	[42]
$CH_3NH_3PbI_3$	mp (TiO_2)	PTAA	16.4	0.90	0.61	9.0	[42]
$CH_3NH_3PbI_3$	mp (TiO_2)	PTAA	19.3	0.91	0.70	12.3	[32]
$CH_3NH_3Pb(I_{1-x}Br_x)_3$	Mesoscopic and planar structures	Poly(triarylamine)	19.64	1.11	74.2	16.2	[79]
$CH_3NH_3PbI_3$	Mesoscopic TiO_2	Spiro	1.02	21.2	77.6	16.7	[80]
$FAPbI_3$	Mesoscopic TiO_2	Spiro	1.03	20.97	74	16	[78]
$CH_3NH_3PbI_{3-x}Cl_x$	Planar heterojunction	Spiro	1.13	22.75	75.01	19.3	[81]
$CH_3NH_3PbI_3$		FDT	1.148	22.7	0.76	20.2	[55]

Abbreviations: mp, mesoporous; spiro, spiro OMeTAD.

Table 3. comprehensive summary of the performance of perovskite solar cells, including the perovskite materials, photoanodes, hole-transport materials (HTMs), J_{SC} (mA/cm), V_{OC} (v), FF and PCE (%)

of both electrons and holes. Now the challenge is to determine whether mesostructure is essential or the thin-film p-i-n can lead to a better performance [76].

2.1.3. Perovskite thin films

While using the methylammonium lead halide ($CH_3NH_3PbX_3$, X-halogen) and its mixed-halide crystals, corresponding to the 3D perovskite structures as light harvesters in solar cells,

it is observed that substituting the I with Cl/Br ions, bandgap tuning of $MAPbX_3$ is achieved, which occurred due to the strong dependence of electronic energies on the effective exciton mass [76]. The entire visible region was controlled by tuning the bandgap. Apart from that, the addition of Cl/Br into an iodide-based structure shows a drastic improvement in the charge transport, relative stability, and separation kinetics within the perovskite layer [77]. It was also observed that the bandgap is reduced (1.48–2.23 eV), leading to high short-circuit currents of >23 mA/cm^2 and a PCE of up to 14.2%, when the cation size of perovskite materials is increased [42].

There are a few solution-based techniques that has been used for the fabrication of thin films, where a mixture of two precursors is used to form final absorber, but due to the lack of suitable solvents and high-reaction rate of the perovskite component, the process results in thin film with pinhole formation and incomplete surface coverage, which deteriorates the film quality and thus effect the device performance.

The two-step deposition technique that was used previously to prepare the films of organic-inorganic systems has incompatible solubility characteristics where the organic component is difficult to evaporate. Devices based on the planar $CH_3NH_3PbI_3$ thin film via the modified two-step deposition technique have also achieved the efficiency of 12.1% [78].

Another technique that was developed was dual-source vapor-deposited organometallic trihalide perovskite solar cells based on a p-i-n thin-film architecture with high efficiency. However, the deposition with the vacuum evaporation method will make it cost effective [26].

2.1.4. Hole-transporting materials (HTMs)

The conductivity of perovskite is high, which requires a thick layer of HTM to avoid pinholes. Spiro-OMeTAD, due to being less conductive, offers high resistance because of thick capping layers. A wide variety of polymer hole conductors are also used, which is shown in **Figure 4**. Protic ionic liquids (PILs) are used as effective p dopants in hybrid solar cells [78] based on triarylamine hole-transporting materials. Further, the efficiency is improved by replacing the lithium salts, p-dopants for spiro-OMeTAD with PILs [79]. While using other HTMs as P3HT and DEH HTM, the efficiency of spiro-OMeTAD is much slower than P3HT and DEH HTM, respectively. However, a recent synthesis based on the pyrene-based derivative Py-C also exhibited an overall PCE of 12.7% [76]. As the hole conductors, spiro-OMeTAD and P3HT are costly, so an inexpensive, stable, solution-processable inorganic CuI as the hole conductor has been demonstrated [80]. A solution-processed p-type direct bandgap semiconductor $CsSnI_3$ with a perovskite structure can also be used for hole conduction replacing a liquid electrolyte [34]. Overall we can say that perovskite materials play both the role of light harvesters and hole conductors. Recently, a hole-conductor-free mesoscopic $CH_3NH_3PbI_3$ perovskite/TiO_2 heterojunction solar cell has reported with a PCE of 5.5% [30], yet the photovoltaic performance was inferior to that of HTM. The tuning of bandgap of perovskite materials plays an important role in photophysical properties. The energy bandgaps of different hybrid materials and the hole-transporting materials are given in **Figures 5** and **6**.

http://dx.doi.org/10.5772/65052

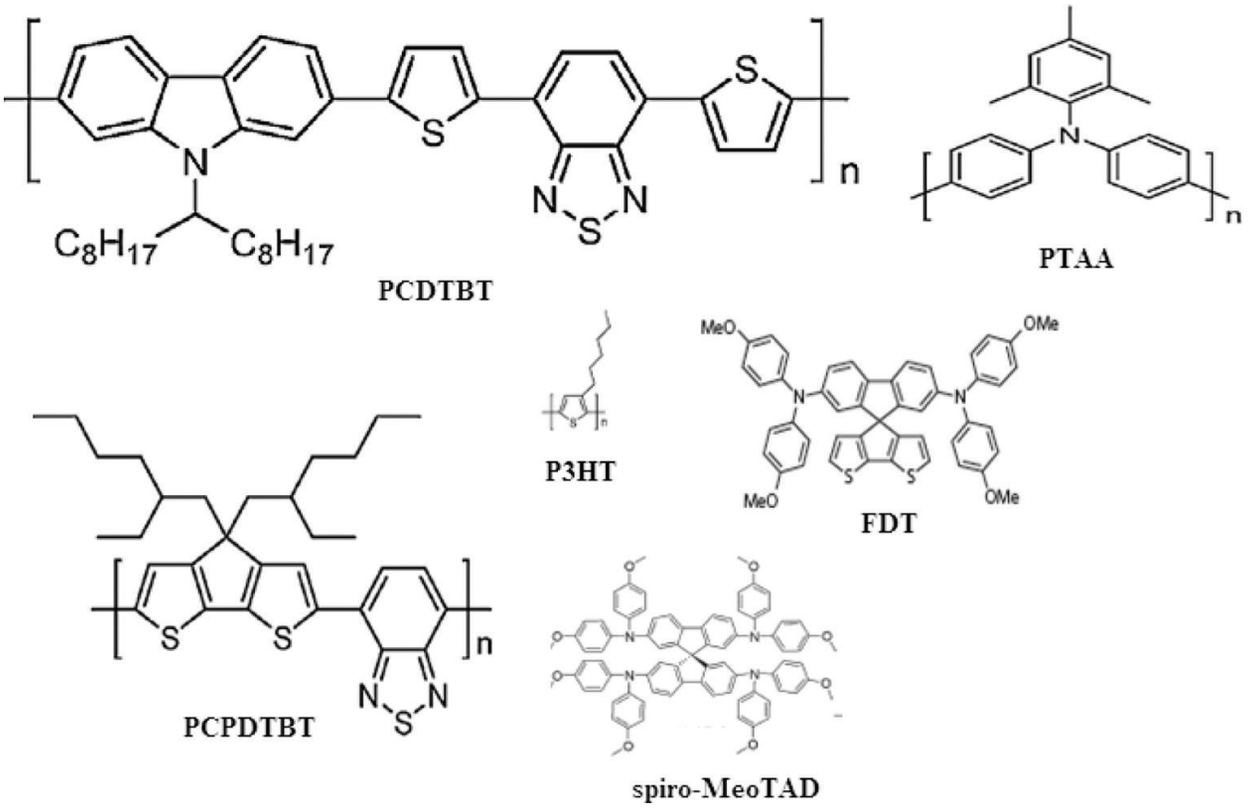

Figure 4. Structural representation of hole-transporting materials (HTMs).

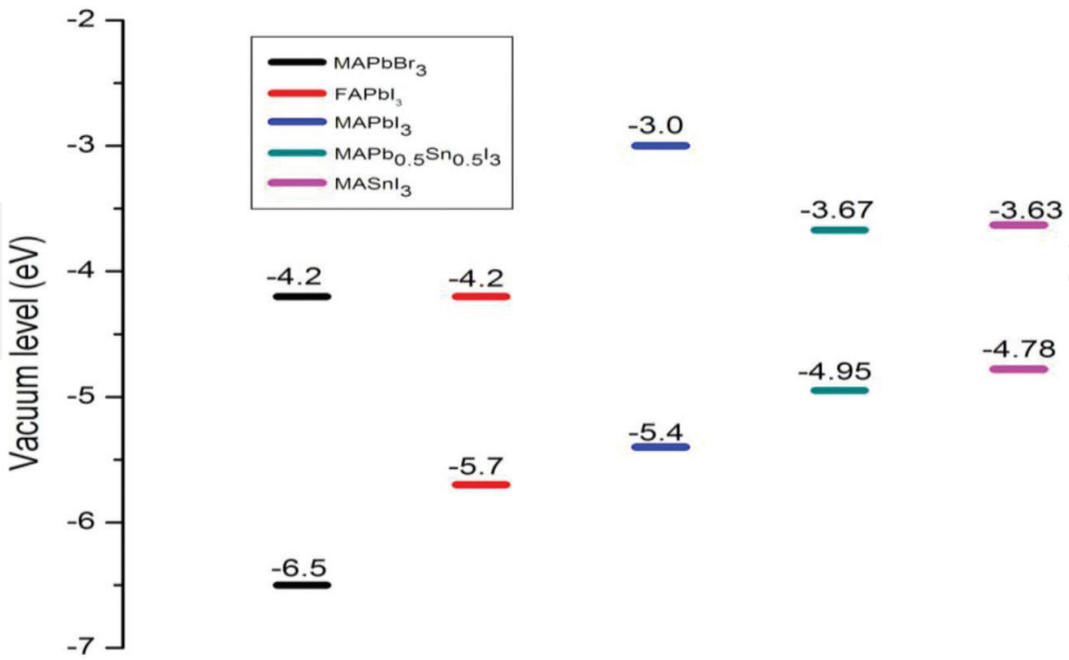

Figure 5. Energy bandgap diagram of hybrid perovskite materials.

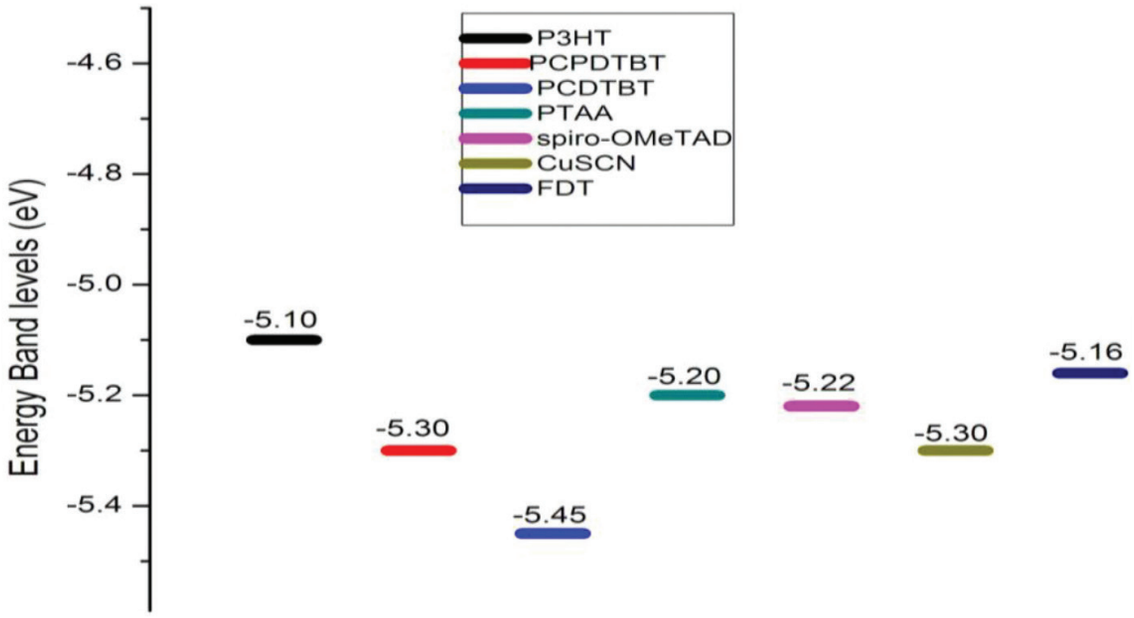

Figure 6. Energy level diagram of hole transporting materials (HTMs).

2.1.5. Measurement of charge-carrier mobility, lifetime and diffusion lengths

Regarding the exciton or the electron and hole diffusion length, it was observed that 100-nm long range diffusion length was obtained in solution-processed $CH_3NH_3PbI_3$ by applying femtosecond transient optical spectroscopy to bilayers that interface this perovskite with either selective-electron or selective-hole extraction materials [38]. The higher efficiency of these materials is only due to the comparable optical absorption length and charge-carrier diffusion lengths. Photoluminescence quenching measurements were performed to extract the electron-hole diffusion lengths in triiodide ($CH_3NH_3PbI_3$) and mixed-halide ($CH_3NH_3PbI_{3-x}Cl_x$) perovskite thin films [39]. In mixed-halide perovskite cells, the larger diffusion length is due to the much longer recombination time, requires both low recombination rates and high charge-carrier mobility; however, the mechanism causing the extended diffusion length is still unclear. Few other things that remain unclear is the relative fraction of free and bound charge pairs at room temperature, the nature of the excited state, and the role of the two species [81, 82].

2.2. Theoretical scenario

There are reports that prove that Density functional theory (DFT) calculations have already carried out before the first perovskite solar cell was reported experimentally [4, 13]. Various theoretical methods were adopted using exchange-correlation functionals such as Local density approximation (LDA) [83], Generalized gradient approximation (GGA) [51], hybrid functional methods (HSE), quasiparticle GW methods, spin-orbit-coupling (SOC), and van der Waals interactions. LDA underestimates and GGA overestimates the lattice parameters.

It is observed that when dispersion interactions are included, the calculated results match well with the experimental results. It is found that adding dispersion corrections increases the binding and corrects the GGA errors.

However, the defects does not affect much as they do not create a detrimental deep level within the bandgap [84, 85] that could be carrier traps and recombination centers for electron-hole in solar cells. Ringwood [86] has included that the contribution of charges depends on the differences in electronegativity. Since lead is considered as a provider of the charge and size, it holds the perovskite crystals all together.

2.2.1. Ambipolar activities

The ambipolar activities of these materials can be defined by taking effective mass into consideration which is defined by formula:

$$m^* = \hbar^2 \left[\frac{\delta^2 \varepsilon(k)}{\delta^2 \varepsilon(k)} \right]^{-1} \tag{3}$$

where $\varepsilon(k)$ is the energy dispersion relation functions, described by the band structures. If the band is more dispersive (flat), near the band edges, the effective mass is lighter (heavier). In perovskite materials, the lone-pair Pb s electrons play a vital role. The electronic structure of $CH_3NH_3PbI_3$ is inverted. The conduction band matrix is derived from Pb p orbitals, and the valence band matrix is a mixture of Pb s and I p (s-p semiconductor) orbitals. A cation Pb p orbital has a much higher energy level than anion p orbitals, although the CBM is derived from Pb p orbitals, Therefore, the lower conduction band of $CH_3NH_3PbI_3$ is more dispersive than the upper valence band, similarly the upper valence band of $CH_3NH_3PbI_3$ is dispersive due to the strong s-p coupling around the Valence band maximum (VBM). Due to the balance between the hole effective mass and the electron effective mass, $CH_3NH_3PbI_3$ leads to higher ambipolar activities. It might be possible that many-body effect plays a role for small carrier effective mass, as the effective mass calculated by the GW + SOC method [87] is even lower. The effective hole and electron masses are given in **Table 4**.

Materials	m_e^*/m_0	m_h^*/m_0	**Bandgap (eV)**
Silicon	0.26	0.29	1.11
GaAs	0.07	0.34	1.43
$CsSnI_3$	0.19	0.09 (0.15)	1.14
$CsSnI_3$ (SOC)	0.16	0.07	
$CH_3NH_3PbI_3$	0.35 (0.32)	0.31 (0.36)	1.5–2.0
$CH_3NH_3PbI_3$ (SOC)	0.18 (0.23)	0.21 (0.29)	

Table 4. Calculated effective masses (electron and holes) and bandgap (eV) for different materials. Experimental values are in parenthesis

2.2.2. Optical absorption spectra

The optical absorption spectra of perovskite materials are determined by the energy bandgaps and partial density of states (pdos). The pdos graph for different materials is depicted in **Figure 7**. The energy bandgap measures the probability of each photoelectric transition and the density of states measures the total number of possible photoelectric transitions. Thus, we can easily conclude that the optical absorption coefficient of a material is closely related to its electronic structure. However, the effect of optical absorption spectra is not considered in the Shockley-Queisser limit [42]. The theoretical maximum efficiency depends on the thickness of the absorber layer. Recently, a method has been developed by Yu et al. [88], in which they calculated the maximum efficiency based on the absorber thickness by taking absorption coefficient and absorber layer thickness both into consideration. So theoretical calculations were carried out on this basis and it was found that halide perovskites ($CH_3NH_3PbI_3$ and $CsPbI_3$) exhibit much higher conversion efficiencies for any given thickness. These materials are also capable of achieving high efficiencies with very thin absorber layers. On the basis of experimental calculations, it is proved that $CH_3NH_3PbI_3$ perovskite has the capability of achieving a high fill factor. Improved interfaces and contact layers also improve the performance of a solar cell, while Pb chalcogenides exhibit abnormal bandgap changes with lattice constant and strain [89].

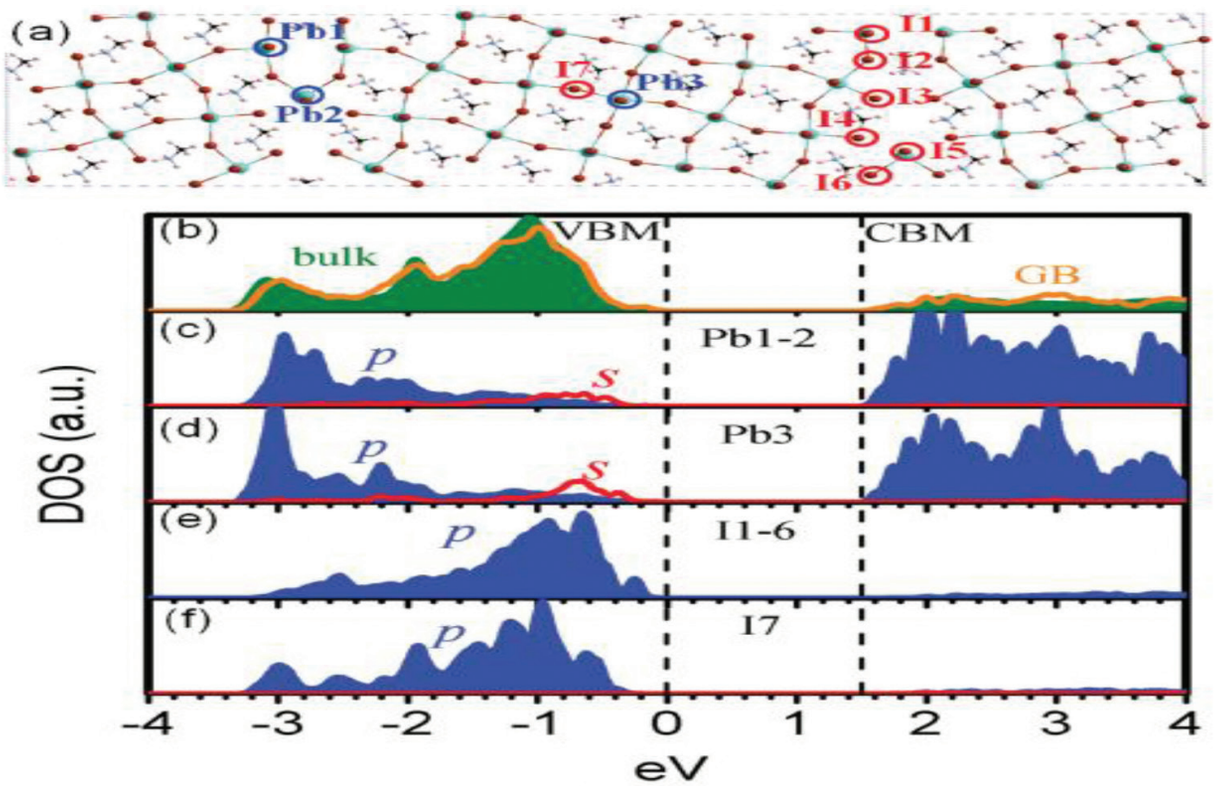

Figure 7. (a) The periodic structural model of Σ5 (310) GB for $CH_3NH_3PbI_3$. (b) Comparison of DOS of bulk $CH_3NH_3PbI_3$calculated from unit cell. (c–f) pdos of selected atoms highlighted in the above structure. Adapted with permission from reference [137].

2.2.3. Ferroelectricity

One more theoretical aspect is the dipole moment of the noncentrosymmetric organic cation in perovskite materials. It was shown from electric dipole calculations of the organic cation that hybrid perovskites exhibit spontaneous electric polarization, which might be due to the two reasons: the alignment of the dipole moments of organic cations and the intrinsic lattice distortion breaking the crystal centrosymmetry. On the basis of this concept, it was proposed in the studies that the presence of ferroelectric domains will result in internal junctions might support electron-hole separation and transportation. However, the calculated value of $CH_3NH_3PbI_3$ bulk polarization is 38 mC/cm^2, which is comparable to the value of ferroelectric oxide perovskites such as $KNbO_3$ (30 mC/cm^2) [90]. Frost and coworkers [91] suggested that it may be possible that the boundaries of ferroelectric domains may form "ferroelectric highways" that facilitate the transportation of electrons and holes. Furthermore, it was proposed that the favorable highways are energetically chosen in such a way that the holes and electrons avoid any collision with the opposite charges. It is directly seen in the recent experiment by direct observation of ferroelectric domains in the β phase of $CH_3NH_3PbI_3$. Another important factor is that V_{OC} can be larger than the bandgap, and charge separation and carrier lifetime can be enhanced due to the internal electric field [92].

2.2.4. Interface and surface

The surface and interface between the absorber, carrier transport layers, and electrode contact layers are also important for efficient carrier transportation. However, the two-step method, vacuum deposition and vapor-assisted solution processing methods [85], have improved the quality much better by the one-step method. The vacuum deposition method is used in small molecule-based devices, which makes the use of insoluble materials more stable than their soluble analogues. There are at least three aspects worth consideration.

2.2.4.1. Band alignment

The bandgaps and band alignments of perovskites can also be tuned by the chemical management of compositional elements, including organic cations [93, 94], Pb [95–97], and halogen elements [98, 99]. This is another way to optimize band alignment at interfaces.

2.2.4.2. Interface structure and passivation

The unusual hysteresis of the *I–V* curve of perovskite solar cells, which would reduce the working cell efficiency, was suspected to be related to the interface properties [99, 100].

2.2.4.3. Surface

Abate et al. [79] reported the existence of trap states at the perovskite surface, which generated charge accumulation and consequent recombination losses in working solar cells. They identified under coordinated iodine ions as responsible and used supramolecular halogen bond complexation for passivation.

2.2.5. Point defects

The p- or n-type absorbers were made from materials with intrinsic defects, or using intentional doping intrinsic defects that create deep energy levels in the absorber usually act as Shockley-Read-Hall nonradiative recombination centers and carrier traps, reducing the carrier lifetime and thus V_{oc}. A good solar cell absorber must exhibit proper doping and defect properties. There are many types of defects as a donor and acceptor which lies in the semiconductors. The formation energy of a defect depends on the chemical potential and environmental factors such as precursors, partial pressure, and temperature. So we can conclude that these experimental conditions play a vital role to determine the formation energies of all the possible defects and further impact the polar conductivity in these materials. Defect formation energies determine the polar conductivity of a semiconductor, whereas defect transition levels determine the electrical effect of any particular defect [101].

Besides point defects, Kim et al. [102] used DFT-GGA to calculate the DOS and partial charge densities of two types of neutral defects in β phase $CH_3NH_3PbI_3$: (a) Schottky defects (equal numbers of positive and negative vacancies) and (b) Frenkel defects (equal numbers of vacancies and interstitials of the same ion). The tunable polar conductivity and shallow defect properties may help to explain why high-performance perovskite solar cells, with extremely long carrier lifetimes [40, 103] can be produced by a diverse range of growth approaches and a wide variety of solar cell architectures. These point defects would suggest new methods for perovskite solar cell architecture. It was observed that deep point defect levels could exist through large atomic relaxations, which is attributed to the strong covalency of the system [104].

2.2.6. Structural disorder

In a recent investigation, Choi et al. [105] found that most of $CH_3NH_3PbI_3$ (70%) is highly disordered with a local perovskite structure extending over a range of only 1.4 nm, which is about 2 lattice constants of the α phase [106].

The mesoporous scaffold confined need the perovskite within the pores and reshaped the structures of perovskites. On the other hand, the low-temperature growth process inevitably leads to polycrystalline perovskites with grain boundaries (GBs). Experimentally, it is very difficult to investigate the structural and electronic properties directly, as it requires a high resolution transmission spectroscopy (HRTEM). So, we have to rely on the theoretical calculations that can give direct insights into the electrical properties of structural disorders and topological defects in hybrid perovskites. Recent combined theoretical and experimental studies [106] have demonstrated that Cl segregated into the GB part of polycrystalline CdTe solar cells effectively taming the detrimental effects at GBs.

Due to the structural complicity of $CH_3NH_3PbI_3$, the GB structures were constructed based on $CsPbI_3$. It was observed that the DOS of the supercells with GBs are very similar to those of single-crystal phases. None of these GBs introduce defect states within the bandgap region. The GW band structure diagram is given in **Figure 8**.

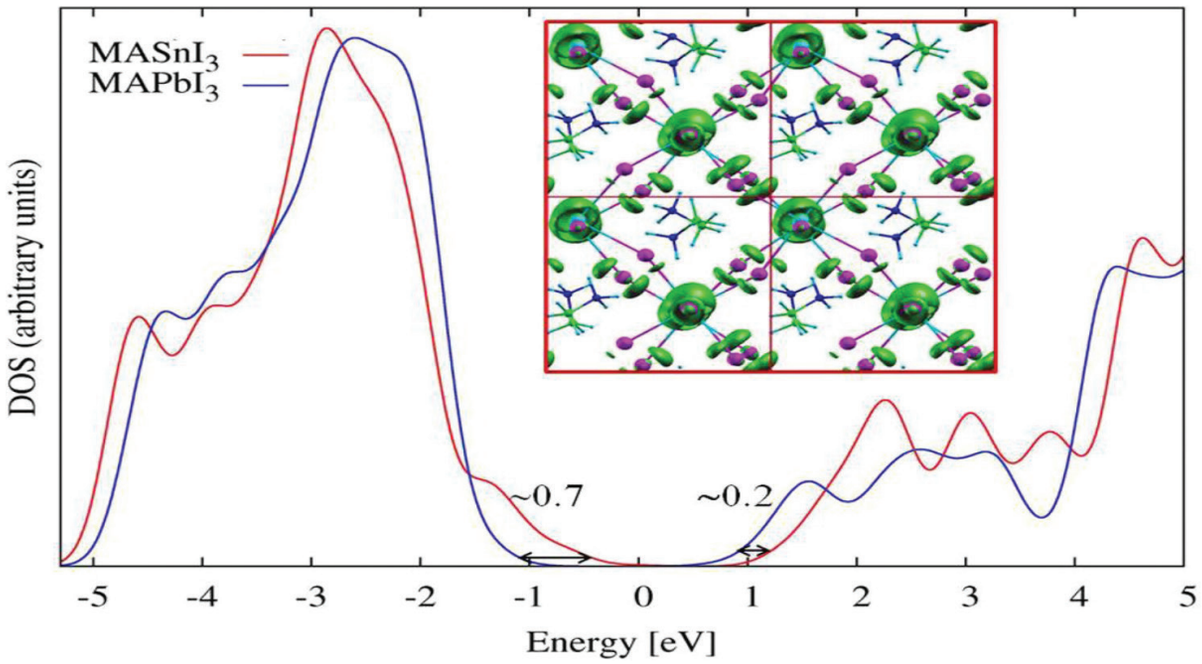

Figure 8. DOS graph of $MASnI_3$ and $MAPbI_3$materials. Adapted with permission from reference [116].

3. Properties

3.1. Electrical properties

Hybrid perovskites exhibit unprecedented carrier transport properties that enable their stellar performance in photovoltaics. So more attention is needed to develop understanding the material properties and ways to improve these properties in all key directions for research. The electrical properties of perovskite materials are seen in the ambipolar carrier transport behavior and long carrier lifetime. These electrical properties are further investigated on the basis of corresponding device structure.

3.1.1. Intrinsic electrical properties

The electrical characteristics of the materials are determined by the carrier type, concentration, and mobility, which is dependent on the method of preparation. It is necessary to use smooth and uniform films to perform measurements. The carrier type is determined by Hall measurements of the conductivity's response to an applied magnetic field, thin-film transistor's response to a gating electric field, and thermoelectric measurements of the Seebeck coefficient. For example, $CH_3NH_3PbI_3$ indicated n-type conductivity, a carrier concentration of ~109 cm^{-3}, and an electron mobility of 66 $cm^2/V/s$ [24]. Carrier concentration can also be adjusted by tuning the stoichiometry of the precursors during solution-phase synthesis and even switch the carrier type to the p-type when excess CH_3NH_3I is used in two-step synthesis.

The electron concentration was measured to be ~1017–1018 cm^{-3}, and it was proposed that the iodide vacancies are responsible for the n-type conductivity [107]. The electron mobility for n-type films deposited from stoichiometric precursors was determined to be 3.9 $cm^2/V/s$ from the Hall measurements, although $CH_3NH_3SnI_3$ prepared by a solid-state reaction in a vacuum-sealed tube showed an electron mobility of 2320 $cm^2/V/s$ [24], while solution processed material measured mobility of 200 $cm^2/V/s$. It was observed that the electron mobility of polycrystalline $CH_3NH_3PbI_3$ films is larger than the thin-film mobility of polymers [107, 108] and colloidal quantum dots (10^{-3}–1 $cm^2/V/s$) [109] comparable to CdTe (10 $cm^2/V/s$) [110] CIGS, Cu_2ZnSnS_4 (CZTS) (10–10^2 $cm^2/V/s$) [111, 112], and polycrystalline Si (40 $cm^2/V/s$) [101]. Film morphology plays an important role as the dark and light conductivities of $CH3NH_3PbI_{3-x}Cl_x$ deposited on a planar scaffold on mesostructured aluminum oxide are quite different [113]. To further increase the photovoltaic performance and radiative lifetime, solvent annealing has been applied to increase the grain size of the films to ~1 μm [114].

3.1.2. Extrinsic electrical properties:

The techniques used to measure the electrical parameters are given in subsections.

3.1.2.1. Impedance spectroscopy (IS) [115, 116]

This technique is used to identify the frequency dependence of capacitance, to measure charge diffusion lengths and lifetimes and to investigate carrier trapping and recombination. The carrier diffusion length was derived and has been estimated to be about ~1 μm for $CH_3NH_3PbI_{3-x}Cl_x$ [83].

3.1.2.2. Electron beam-induced current (EBIC) [117]

Another method to obtain the electrical parameters is EBIC from which the calculated carrier diffusion length for$CH_3NH_3PbI_{3-x}Cl_x$ is 1.5–1.9 μm [40]. The carrier diffusion length is comparable or longer than that of other polycrystalline semiconductors with direct bandgaps used in solar cells [76, 77, 118–120]

3.2. Optical properties

It is very important to understand the optical response of the materials, as optical properties are the most important feature of perovskite materials and they provide insights into the electronic and chemical structures. The ability to tune the optoelectronic properties with ease presents a major attraction among researchers. Few important parameters that are used to define these properties are discussed herein:

3.2.1. Optical constants

A lot of research has been conducted on tuning the bandgap of perovskite, but a more detail understanding of these materials awaits further research. The major problem that occurs in perovskite materials is the difficulty of producing continuous films of sufficient smoothness [121] to avoid measurement artifacts from spectroscopic measurements of transmittance,

reflectance, and ellipsometry. The absorption coefficients determined from the absorption of $CH_3NH_3PbI_3$ films on quartz [122] and glass [123] yield values of ~104 cm^{-1} near the band edge without providing any corrections for the surface's inhomogeneity, so for accurate measurements is important to calculate the absorption coefficients based on the optical constants of $CH_3NH_3PbI_3$ [124]. It is observed that the absorption spectrum for $CH_3NH_3PbI_3$ differs, when deposited within a mesoscopic template and planar substrates, which might be due to the changes in the crystallite morphology that affects the optical transitions [125, 126].

3.2.2. Excitons

Exitons play an important role in perovskites. The studies indicate, however, that there is not significant population of excitons in photovoltaics made from $CH_3NH_3PbI_3$, whose exciton-binding energy has been reported between 20 and 50 meV, comparable to the thermal energy at room temperature [127, 128]. These values have been obtained by fitting temperature-dependent absorption spectra using the measured [88] reduced mass of the exciton. Excitonic radius from the binding energy and an appropriate dielectric constant study is still a subject of debate [129]. The excitonic transition significantly enhances the absorption of hybrid perovskites near the band edge [130, 131].

3.2.3. Photoluminescence

The photoluminescence (PL) efficiency depends on the pump fluence. The trapping of photogenerated charges competes effectively with direct radiative recombination of electrons while holes reduce luminescence at low excitation energies. The PL efficiency of$CH_3NH_3PbI_3$is ~17–30%. The PL efficiency falls at higher pumping and high charge carrier densities. The PL lifetime measurements reported shorter lifetime (between 3 and 18 ns) at low pump fluencies [127, 132–134]. These longer lifetimes have been found in a semiconductor in doped and undoped GaAs films. This might be due to the photon recycling and the PL lifetime dependency on surface recombination than radiative recombination. So we can conclude that photon cycling plays a major role in their excited state dynamics, when nonradiative decay pathways are suppressed. The absorption spectra and photoluminescence for perovskite materials are shown in **Figure 9**.

3.2.4. Vibrational spectroscopy

IR spectroscopy also plays an important role in determining the chemical composition. If we look into the chemical structure of $CH_3NH_3PbI_3$, $CH_3NH_3PbBr_3$, and $CH_3NH_3PbCl_3$, the first one is tetragonal, while the other two are cubic. Raman-active modes are precluded in the symmetry of the lattice for cubic structures [135], though a weak broadband at 66 cm^{-1} is observed in $CH_3NH_3PbCl_3$. For $CH_3NH_3PbI_3$, the resonant Raman spectrum (DFT calculations) has been observed with nodes below 100 cm^{-1} (approximately) related to the inorganic octahedron. The higher energy modes indicate the disorder of $CH_3NH_3^+$ cations. A lot of work in this field is still required to investigate how the modes shift occurs with the structural changes. Raman nodes can provide better tool in understanding the in homogeneity of perovskite films with submicron spatial resolution.

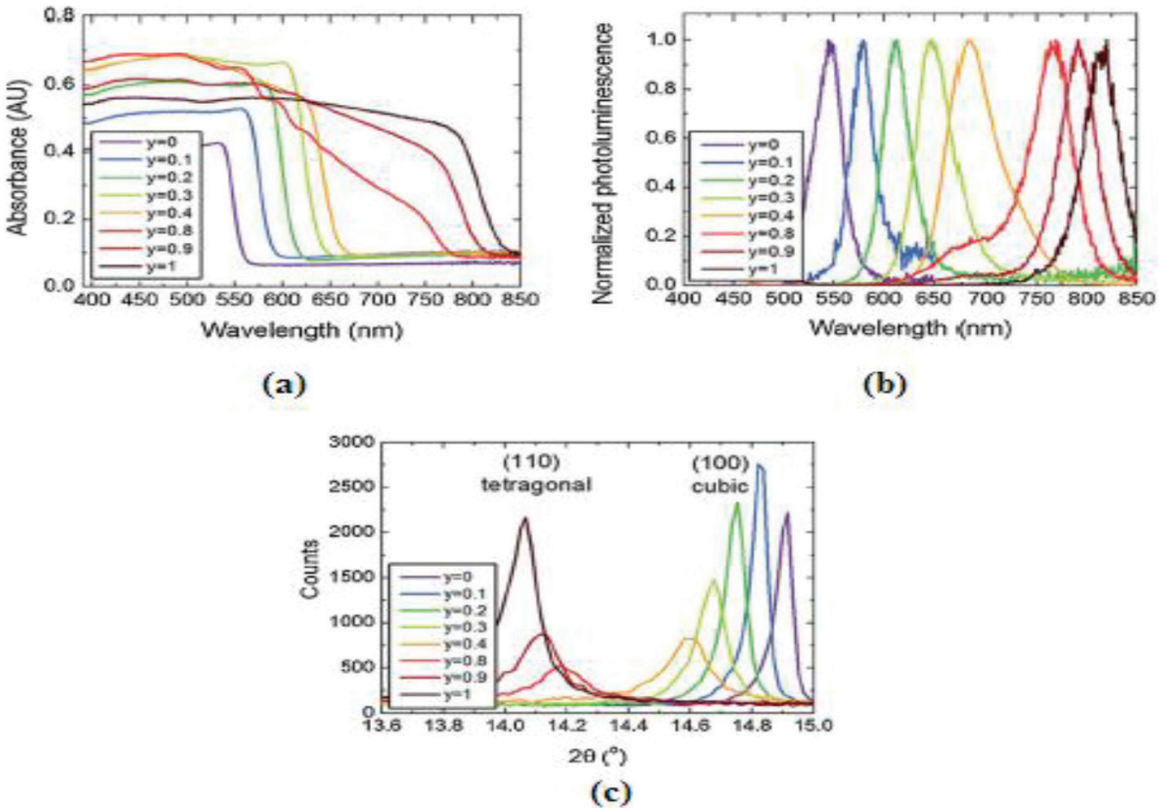

Figure 9. (a) Absorption spectra, (b) photoluminescence spectra of $FAPbI_xBr_{3-x}$ (varying I:Br ratio), (c) XRD spectra of the phase transition Br-rich cubic phase to the I-rich tetragonal phase. Adapted with permission from reference [37].

4. Pitfalls

4.1. Hysteresis

Perovskite solar cells exhibit an anomalous hysteresis in the current-voltage and resistivity-temperature dependence curves [136]. Though it was predicted that the hysteresis on resistivity verses temperature curves is associated with the structural phase transition while the reason for current-voltage curves are still unknown. In an extensive [E-CE6] studies carried out by Prof. Erik Christian Garnett et al. [136], several explanations have been proposed as ion migration, filling of interface, or surface trap states, accumulation of charges at grain boundaries and ferroelectricity, yet no convinced conclusion has been drawn. In structural perception, the cubic phases of the chloride and bromide perovskites do not allow a polar ferroelectric distortion. Various hypotheses have been suggested and it was further predicted that hysteresis should depend on the magnitude of the dipole moment of the organic cationic species and the connecting halide cage. Though the origin of this phenomenon is not yet understood properly, a number of possible causes have been proposed in which the noted causes are ferroelectricity or the presence of mobile ionic species [136]. The illustration for the hysteresis in the electrical transport in hybrid perovskites is given in **Figure 10**.

Here, it is necessary to mention that reporting results from single *J–V* sweeps, even in the absence of hysteresis, or choosing scan rates to report the highest efficiencies, will lead to

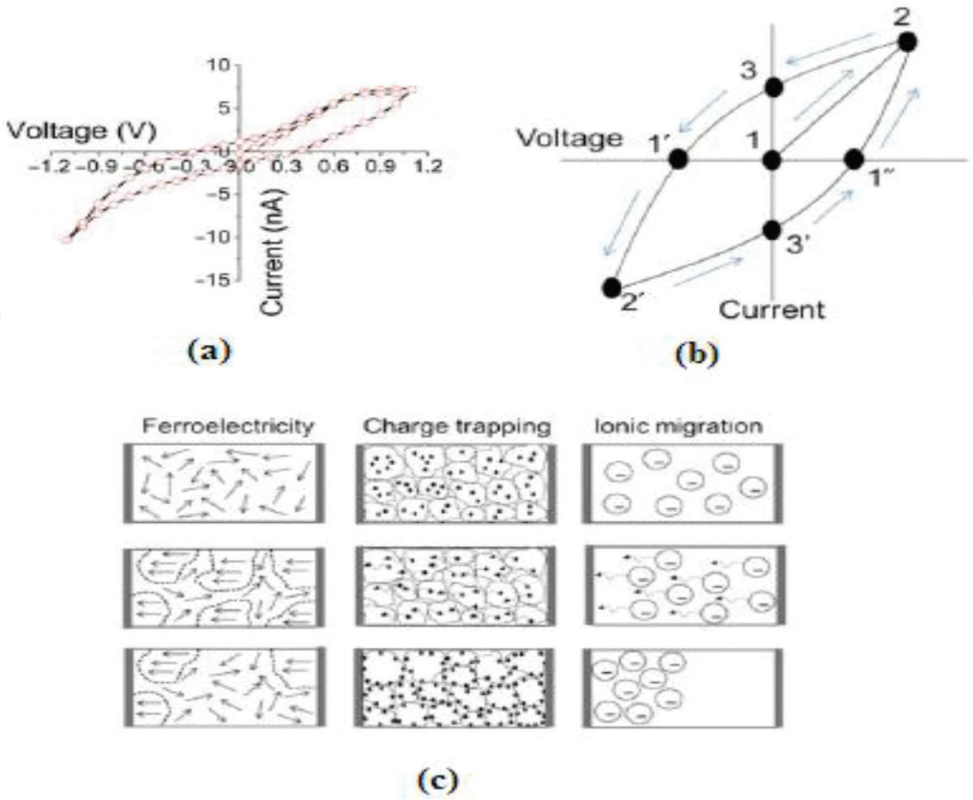

Figure 10. Hysteresis representation in hybrid perovskites. (a) *I-V* graph of $CH_3NH_3PbI_3$ (single crystal) at room temperature, (b) schematic *I-V* curve, (c) proposed phenomena for its origin. Adapted with permission from reference [104].

misleading results. As it might be possible that the certified efficiencies for perovskite solar cells are deemed "not stabilized" though they were measured with negligible hysteresis.

4.2. Thermal and operational stability

There are so many reports that claim that perovskite solar cells have been shown to be stable for many hundreds of hours without any encapsulation. However, the solar cells were stored in the dark and only measured occasionally. So we can conclude that the sealing from environmental ageing is necessary because of operation at elevated temperature and humidity. Stability has become a bigger problem for tin (II) perovskites due to the decrease in stability of the oxidation state of tin (II) compare to lead (II).

4.3. Toxicity

Due to the toxic nature of lead, concerns have been raised on the possible environment and legalization problems from perovskite solar cells based on water soluble lead compounds. So efforts have been made to replace lead with other metal ions without degrading the photophysical properties with quantum mechanical calculations. As lead halogen perovskites are water soluble, the most pessimistic view is the consequences of damaged solar cells and panels with potential exposure to water followed by dissolution and distribution of lead ions into buildings, soil, air, and water.

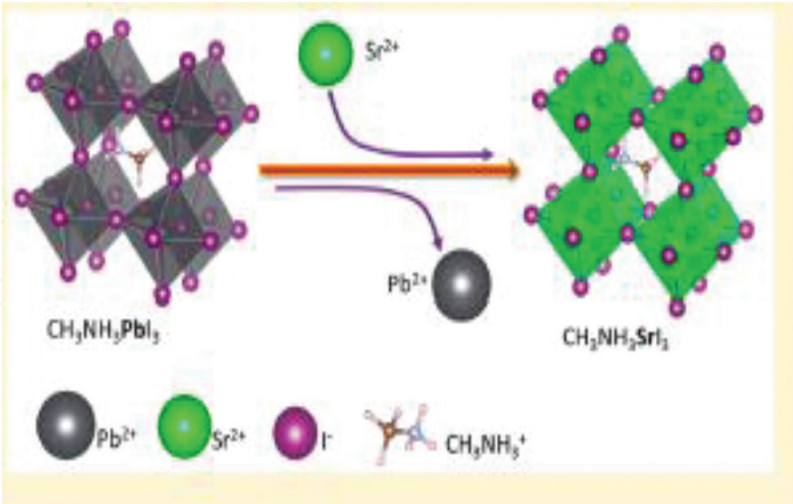

Figure 11. Pictorial representation of replacement of lead by strontium in perovskite solar cells [138].

Lead is known to damage the nervous system and cause brain disorders. In this direction, a theoretical study carried out by De Angelis and group [137] has replaced Pb by Sn (**Figure 11**) with effective development of the GW method with spin-orbit coupling to accurately model the properties of $CH_3NH_3SnI_3$ and then compared it to the $CH_3NH_3PbI_3$. They predicted that $MASnI_3$ is a better electron transporter than $MAPbI_3$ by the SR-DFT method. Another study carried out by Jesper Jacobsson and group [138] has provided deep physical insights into the photophysical nature of a metal-halogen perovskite by removing lead with strontium, which is relatively nontoxic and inexpensive. CCSD calculations and DFT study were performed on the two basic structures of $CH_3NH_3SrI_3$ and $CH_3NH_3PbI_3$ to extract and compare the electronic structures and the optical properties. This is based on the fact that the ionic radii of Sr^{2+} and Pb^{2+} are almost identical, so the exchange could be made as it will not affect the crystal structure. $CH_3NH_3SrI_3$ gives a bandgap of 1.6 eV, which is fairly close to the experimental value reported to be around 1.55 eV [5, 42]. The second effect that was caused by shifting Sr for Pb is that the shape of the pdos graphs for both the halogen and the organic ion is shifted and slightly distorted. The lower electronegativity of Sr compared to Pb shifts the electronic cloud closer to the iodine atoms in the lattice, which perturb the local dipole moment as well as the bonding angles between the iodine octahedra and consequently their columbic interaction with the methylammonium dipoles. The charge distribution is similar to the two structures, with higher charge density around lead compared to strontium due to the higher atomic number of lead.

5. Roadmap

The Perovskite solar cell (PSC) field has now become an emerging field and reports on further improvement in performance are expected in the near future, achieving PCE of more than 30% efficiency has now become a realistic goal. Furthermore, PSC can be used as top cells in two-level tandem configurations using crystalline silicon or copper indium gallium

selenide-based photovoltaic devices as bottom cells. It is expected that by using silicon-based tandems, PCEs of 28–30% can be achieved. Yet there are issues related to the stability and toxicity, hysteresis in perovskite solar cells, which has to be solved. Experimental and theoretical investigations have demonstrated that that halide perovskites exhibit a series of superior electronic and optical properties for solar cell applications, such as proper band-gap and band alignment, high optical absorption, bipolar carrier conductivity, tunable doping ability, and benign defect properties. A lot of studies are required to optimize the material properties and to find new perovskite candidates for high-efficiency, stable solar cells. Band structure engineering of $CH_3NH_3PbI_3$ needs to be extensively investigated by replacing organic cations, Pb or I, with other choices. Furthermore, the mechanisms of performance degradations have to be resolved in a more prominent manner. Water-corroded perovskites as rapid degradation occur in moist environments. So the reaction mechanism between H_2O and the perovskite surface could be carefully studied, leading to the development of new methods for stabilizing perovskites. Although some groups have fabricated the long-term stable perovskites in the laboratory through chemical composition engineering [32, 88], the fundamental reason for alloy stabilization of the structures requires more study. However, it is predicted that the study should converge to the p-i-n planar heterojunction perovskite solar cell to understand the device structure and properties from single crystal.

6. Conclusions

The intense appeal of hybrid organic-inorganic perovskite materials such as solar cells is exceptionally promising. Their enhance optoelectronic properties, deposition techniques, and device structure have led to the higher power conversion efficiencies. Due to the high absorption coefficients and panchromatic absorptions of perovskite, they have become ideal materials for thin film solar cells. However, some complexities as the poor stability in humid air and the toxicity of lead used are a matter of concern. In some perovskite materials, the hysteresis is also pronounced due to the strong dependence of photocurrent to the voltage scan conditions. Still the exceptional performance of hybrid perovskite materials has created revolution in the field of renewable energy with cheap solar cells. Highly efficient solar cells with record performance are still an important milestone to be achieved. The highly innovative and new elegant designs, deep insights into the photophysics and mechanisms of cell operation should now be the main focus of future research.

Finally, we can conclude that the recent advances with perovskite materials will motivate the researchers to expand their horizons to other inorganic or organic pigments, for which the power of mesoscopic solar-cell architectures will emerge to offers more promising opportunities.

The author acknowledges the financial assistance by the DST WOS-A (CS-1005/2014). The author is also thankful to her mentors Dr. G. Narahari Sastry, Head, Center for Molecular Modeling and Dr. K. Bhanuprakash, Chief Scientist, I& PC division, CSIR-Indian Institute of Chemical Technology for the useful discussions and suggestions.

Author details

Ruby Srivastava

CSIR-Indian Institute of Chemical Technology

Hyderabad, Telangana State, India

References

[1] Darling B, You FQ, Veselka T, Velosa A. Assumptions and the levelized cost of energy for photovoltaics. Energy and Environmental Science. 2011;4:3133–3139. DOI: 10.1039/c0ee00698j.

[2] Yue DJ, Khatav P, You FQ, Darling SB. Deciphering the uncertainties in life cycle energy and environmental analysis of organic photovoltaics. Energy and Environmental Science. 2012;5:9163–9172. DOI: 10.1016/j.solmat.2011.08.025.

[3] Ginley D, Green MA, Collins R. Solar energy conversion toward 1 terawatt. MRS Bulletin. 2008;33:355–364. DOI: 10.1557/mrs2008.

[4] Chen X, Jia BH, Zhang YN, Gu M. Exceeding the limit of plasmonic light trapping in textured screen-printed solar cells using Al nanoparticles and wrinkle-like graphene sheets. Light: Science and Applications. 2013;2:e92. DOI: 10.1364/OME.3.000489.

[5] Hibberd CJ, Chassaing E, Liu W, Mitzi DB, Lincot D. Non-vacuum methods for formation of $Cu(In,Ga)(Se,S)_2$ thin film photovoltaic absorbers. Progress in Photovoltaics Research and Applications. 2010;18:434–452. DOI: 10.1002/pip.914.

[6] Samuel SD, Snaith HJ. Metal-halide perovskites for photovoltaic and light-emitting devices. Nature Nanotechnology. 2015;10,391–402. DOI: 10.1039/C4MH00238E.

[7] Robert WM, Guillaume Z, Ian F. Inorganic photovoltaic cells. Materials Today. 2007;10(11):20–27. DOI: 10.1007/BF03353779.

[8] Hagfeldt A, Boschloo G, Sun LC, Kloo L, Pettersson H. Dye-sensitized solar cells. Chemical Review. 2010;110:6595–6663. DOI: 10.1021/cr900356p.

[9] Cong JY, Yang XC, Kloo L, Sun LC. Iodine/iodide-free redox shuttles for liquid electrolyte-based dye-sensitized solar cells. Energy and Environmental Science. 2012;5:9180–9194. DOI: 10.1039/C2EE22095D.

[10] Tetreault N, Grätzel M, Novel nanostructures for next generation dye-sensitized solar cells. Energy and Environmental Science. 2012;5:8506–8516. DOI: 10.1039/C2EE03242B.

[11] Boschloo G, Hagfeldt A. Characteristics of the iodide/triiodideredox mediator in dye-sensitized solar cells. Accounts of Chemical Research. 2009;42:1819–1826. DOI: 10.1021/ar900138m.

[12] Yum JH, Baranoff E, Kessler F, Moehl T, Ahmad S. A cobalt complex redox shuttle for dye-sensitized solar cells with high open-circuit potentials. Nature Communication. 2012;3:631–635. DOI: 10.1038/ncomms1655.

[13] Kojima A, Teshima K, Shirai Y, Miyasaka T. Organometal halide perovskites as visible-light sensitizers for photovoltaic cells. Journal of American Chemical Society. 2009;131:6050–6051. DOI: 10.1021/ja809598r.

[14] Feldt SM, Gibson EA, Gabrielsson E, Sun LC, Boschloo G. Design of organic dyes and cobalt polypyridineredox mediators for high-efficiency dye-sensitized solar cells. Journal of American Chemical Society. 2010;132:16714–16724. DOI: 10.1021/ja1088869.

[15] Xu CK, Wu JM, Desai UV, Gao D. Multilayer assembly of nanowire arrays for dye-sensitized solar cells. Journal of American Chemical Society. 2011;133:8122–8125. DOI: 10.1021/ja202135n.

[16] Law M, Greene LE, Johnson JC, Saykally R, Yang P. Nanowire dye-sensitized solar cells. Nature Materials. 2005;4:455–459. DOI: 10.1038/nmat1387.

[17] Yella A, Lee HW, Tsao HN, Yi CY, Chandiran AK. Porphyrin-sensitized solar cells with cobalt (II/III)-based redox electrolyte exceed 12 percent efficiency. Science. 2011;334:629–634. DOI: 10.1126/science.1209688.

[18] Bach U, Lupo D, Comte P, Moser JE, Weissortel F. Solid-state dye-sensitized mesoporous TiO_2 solar cells with high photon-to-electron conversion efficiencies. Nature. 1998;395:583–585. DOI: 10.1038/26936.

[19] Yang L, Cappel UB, Unger EL, Karlsson M, Karlsson KM. Comparing spiro-OMeTAD and P3HT hole conductors in efficient solid state dye-sensitized solar cells. Physical Chemistry Chemical Physics. 2012;14:779–789. DOI: 10.1039/C1CP22315A.

[20] Zhang W, Zhu R, Li F, Wang Q, Liu B. High-performance solid-state organic dye sensitized solar cells with P3HT as hole transporter. Journal of Physical Chemistry C. 2011;115:7038–7043. DOI: 10.1021/jp064256o.

[21] Tan SX, Zhai J, Wan MX, Meng QB, Li YL. Influence of small molecules in conducting polyaniline on the photovoltaic properties of solid-state dye-sensitized solar cells. Journal of Physical Chemistry B. 2004;108:18693–18697. DOI: 10.1021/jp036786f.

[22] Murakoshi K, Kogure R, Wada Y, Yanagida S. Fabrication of solid-state dye-sensitized TiO_2 solar cells combined with polypyrrole. Solar Energy Materials and Solar Cells. 1998;55:113–125. DOI: 10.3390/ijms11031103.

[23] Krüger J, Plass R, Cevey L, Piccirelli M, Grätzel M. High efficiency solid-state photovoltaic device due to inhibition of interface charge recombination. Applied Physics Letters. 2001;79:2085–2087. DOI: 10.1063/1.1406148.

[24] Bagher AM, Abadi Vahid MM, Mohsen M. Types of solar cells and application. American Journal of Optics and Photonics. 2015;3(5):94–113. DOI: 10.11648/j.ajop.20150305.

[25] Yin WJ, Shi T, Yan Y. Unique properties of halide perovskites as possible origins of the superior solar cell performance. Advance Materials. 2014;26:4653–4658. DOI:10.1002/adma.201306281.

[26] Liu M, Johnston MB, Snaith HJ. Efficient planar heterojunction perovskite solar cells by vapour deposition. Nature. 2013;501:395–398. DOI: 10.1038/nature12509.

[27] Wojciechowski K, Saliba M, Leijtens T, Abate A, Snaith HJ. Sub-150°C processed meso-superstructured perovskite solar cells with enhanced efficiency. Energy and Environmental Science. 2014;7:1142–1147. DOI: 10.1039/C3EE43707H.

[28] Im JH, Lee CR, Lee JW, Park SW, Park NG. 6.5% efficient perovskite quantum-dot-sensitized solar cell. Nanoscale. 2011;3:4088–4093. DOI: 10.1039/c1nr10867k.

[29] Lee MM, Teuscher J, Miyasaka T, Murakami TN, Snaith HJ. Efficient hybrid solar cells based on meso-superstructured organometal halide perovskites. Science. 2012;338:643–647. DOI: 10.1126/science.1228604.

[30] Etgar L, Gao P, Xue ZS, Peng Q, Chandiran AK. Mesoscopic $CH_3NH_3PbI_3/TiO_2$ heterojunction solar cells. Journal of American Chemical society. 2012;134:17396–17399. DOI: 10.1021/ja307789s.

[31] Shin SS, Kim JS, Suk JH, Lee KD, Kim DW. Im-proved quantum efficiency of highly efficient perovskite $BaSnO_3$-based dye-sensitized solar cells. ACS Nano. 2013;7:1027–1035. DOI: 10.1039/c0ee00678e.

[32] Noh JH, Im SM, Heo JH, Mandal TN, Seok SI. Chemical management for colorful, efficient, and stable inorganic–organic hybrid nanostructured solar cells. Nano Letters. 2013;13:1764–1769. DOI: 10.1021/nl400349b.

[33] Bi DQ, Yang L, Boschloo G, Hagfeldt A, Johansson EMJ. Effect of different hole transport materials on re-combination in $CH_3NH_3PbI_3$ perovskite-sensitized mesoscopic solar cells. The Journal of Physical Chemistry Letters. 2013;4:1532–1536. DOI: 10.1021/jz400638x.

[34] Chung I, Lee BH, He JQ, Chang RPH, Kanatzidis MG. All-solid-state dye-sensitized solar cells with high efficiency. Nature. 2012;485:486–489. DOI:10.1038/nature11067.

[35] Kim HS, Lee JW, Yantara N, Boix PP, Kulkarni SA. High efficiency solid-state sensitized solar cell-based on submicrometer rutile TiO_2 nanorod and $CH_3NH_3PbI_3$ perovskite sensitizer. Nano Letters. 2013;13:2412–2417.DOI: 10.1021/nl400286w.

[36] Singh SP, Nagarjuna P. Organometal halide perovskites as useful materials in sensitized solar cells: Dalton Transactions. 2014;43:5247–5251. DOI: 10.1039/c3dt53503g.

[37] Song TB, Chen Q, Zhou H, Jiang CY, Wang HH, Yang Y, Liu YS, You J, Yang Y. Perovskite solar cells: film formation and properties. Journal of Material Chemistry A. 2015;3:9032–9050. DOI: 10.1039/c4ta05246c.

[38] Xing GH, Mathews N, Sun SY, Lim SS, Lam YM. Long-range balanced electron- and hole-transport lengths in organic-inorganic $CH_3NH_3PbI_3$. Science. 2013;342:344–347. DOI: 10.1126/science.1243167.

[39] Stranks SD, Eperon GE, Grancini G, Menelaou C, Alcocer MJP. Electron-hole diffusion lengths exceeding 1micrometer in an organometal trihalide perovskite absorber. Science. 2013;342:341–344. DOI: 10.1126/science.1243982.

[40] Wehrenfennig C, Eperon GE, Johnston MB, Snaith HJ, Herz LM. High charge carrier mobilities and lifetimes in organolead trihalide perovskites. Advance Materials. 2014;26:1584–1589. DOI: 10.1021/acs.accounts.5b00411.

[41] Eperon GE, Stranks SD, Menelaou C, Johnston, Michael MB, Herz, LM, SnaithHJ. Formamidinium lead trihalide: a broadly tunable perovskite for efficient planar heterojunction solar cells. Energy and Environmental Science. 2014;7(3):982. DOI:10.1039/C3EE43822H.

[42] Burschka J, et al. Sequential deposition as a route to high-performance perovskite-sensitized solar cells. Nature. 2013;499:316–319. DOI: 10.1038/nature12340.

[43] Service RF. Turning up the light. Science. 2013;342:794–797. DOI: 10.1126/science.342.6160.794.

[44] Nie W, et al. High-efficiency solution-processed perovskite solar cells with millimeter-scale grains. Science. 2015;347:522–525. DOI: 10.1126/science.aaa0472.

[45] Saliba M, Orlandi S, Matsui T, Aghazada S, Cavazzini M, Correa-Baena JP, Gao P, Scopelliti R, Mosconi E, Dahmen KH, Angelis FD, Abate A, Hagfeldt A, Pozzi G, Grätzel M, Nazeeruddin MK. A molecularly engineered hole-transporting material for efficient perovskite solar cells**.** Nature Energy. 2016;1:15017. DOI: 10.1038/NENERGY.2015.17.

[46] The Hong Kong Polytechnic University. Perovskite-silicon tandem solar cells with the world's highest power conversion efficiency. ScienceDaily. ScienceDaily, 12 April 2016. www.sciencedaily.com/releases/2016/04/160412104814.htm.

[47] McMeekin DP, Sadoughi G, Rehman W, Eperon GE, Saliba M, Horantner MT, Haghighirad A, Sakai N, Korte L, Rech B, Johnston MB, Herz LM, Snaith HJ. A mixed-cation lead mixed-halide perovskite absorber for tandem solar cells. Science. 2016;351(6269):151–155. DOI: 10.1126/science.aad5845.

[48] Bi D, Moon SJ, Haggman L, Boschloo G, Yang L, Johansson EMJ, Nazeeruddin MK, Grätzel M, Hagfeldt A. Using a two-step deposition technique to prepare perovskite (CH3NH3PbI3) for thin film solar cells based on ZrO_2 and TiO_2 mesostructures. RSC Advances. 2013;3:18762–18766. DOI: 10.1039/C3RA43228A.

[49] Borriello I, Cantele G, Ninno D. Ab initio investigation of hybrid organic-inorganic perovskites based on tin halides. Physical Review B. 2008;77:235214–235227. DOI: 10.1103/PhysRevB.77.235214.

[50] Shirane G, Danner H, Pepinshi R. Neutron diffraction study of orthorhombic $BaTiO_3$. Physical Review. 1957;105:856–860. DOI: http://dx.doi.org/10.1103/PhysRev.

[51] Ray SS, Okamoto M. Polymer/layered silicate nanocomposites: a review from preparation to processing. Progress in Polymer Science. 2003;28:1539–1641. DOI:progpolymsci.2003.08.002.

[52] Ray SS, Bousmina M. Biodegradable polymers and their layered silicate nanocomposites: in greening the 21st century materials world. Progress in Materials Science. 2005;50:962–1079. DOI: 10.1016/j.pmatsci.2005.05.002.

[53] Mitzi DB. Synthesis and crystal structure of the alkylbismuth diiodides: a family of extended one-dimensional organometallic compounds. Inorganic Chemistry. 1996;35:7614–7619. DOI: 10.1021/ic961083g.

[54] Stoumpos CC, Malliakas CD, Kanatzidis MG. Semiconducting tin and lead iodide perovskites with organic cations: phase transitions, high mobilities, and near-infrared photoluminescent properties. Inorganic Chemistry. 2013;52:9019–9038. DOI: 10.1021/ic961083g.

[55] Shum K, Chen Z, Qureshi J, Yu CL, Wang JJ. Synthesis and characterization of $CsSnI_3$ thin films. Applied Physics Letters. 2010;96:221903–221906. DOI: 10.1063/1.3442511.

[56] Yamada K, Kuranaga Y, Ueda K, Goto S, Okuda T. Phase transition and electric conductivity of $ASnCl_3$ (A = Cs and CH_3NH_3). Bulletin of the Chemical Society of Japan. 1998;71:127–134. DOI: 10.1021/acs.accounts.5b00229.

[57] Xu Q, Educhi T, Nakayama H, Nakamura N, Kishita M. Molecular motions and phase transitions in solid $CH_3NH_3PbX_3$ (X = Cl, Br, I) as studied by NMR and NQR. Zeitschrift Naturforschung. 1991;46:240–246. DOI: 10.1016/0360-3016(94)90398.

[58] Goldschmidt VM. The laws of crystal chemistry. Naturwissenschaften. 1926;14:477–485. DOI: 10.1007/BF01507527.

[59] Calabrese J, Jones NL, Harlow RL, Herron N, Thorn DL, Wang Y. Preparation and characterization of layered lead halide compounds. Journal of American Chemical Society. 1991;113:2328–2330. DOI: 10.1021/ja00006a076.

[60] Mitzi DB, Wang S, Field CA, Chess CA, Guloy AM. Conducting layered organic-inorganic halides containing (1 1 0)-oriented perovskite sheets. Science. 1995;267:1473–1476. DOI: 10.1126/science.aac7660.

[61] Pauling L. The Nature of the Chemical Bond, 3rd ed. Cornell University Press: New York, 1960. DOI: 10.1021/ja01360a004.

[62] Quarti C, Mosconi E, De Angelis F. Interplay of orientational order and electronic structure in methylammonium lead iodide: implications for solar cell operation. Chemistry of Materials. 2014;26:6557–6569. DOI: 10.1021/cm5032046.

[63] Mitzi DB. Thin-film deposition of organic–inorganic hybrid materials. Chemistry of Materials. 2001;13:3283–3298. DOI: 10.1021/cm0101677.

[64] Valiente R, Rodriguez F. Electron-phonon coupling in charge-transfer and crystal-field states of Jahn–Teller CuCl64-systems. Physical Review B. 1999;60:9423–9429. DOI: 10.1103/PhysRevB.60.6584.

[65] Kagan CR, Mitzi DB, Dimitrakopoulos CD. Organic inorganic hybrid materials as semiconducting channels in thin film field-effect transistors. Science. 1999;286:945–947. DOI: 10.1126/science.286.5441.945.

[66] Zhou P, Drumheller JE, Patyal B, Willet RD. Magnetic properties and critical behavior of quasi-two-dimensional systems $[C_6H_5(CH_2)_nNH_3]_2CuBr_4$ with n = 1, 2, and 3. Physical Review B. 1992;45:12365–12376. DOI: 10.1103/PhysRevB.45.5744.

[67] Era M, Morimoto S, Tsutsui T, Saito S. Organic-inorganic heterostructure electroluminescent device using a layered perovskite semiconductor $(C_6H_5C_2H_4NH_3)_2PbI_4$. Applied Physics Letters. 1994;65:676–678. DOI: 10.1063/1.112265.

[68] Hong X, Ishihara T, Nurmikko AV. Dielectric confinement effect on excitons in PbI_4-based layered semiconductors. Physical Review B. 1992;45:6961–6964. DOI: 10.1063/1.4936776.

[69] Kim HS, Lee CR, Im JH, Lee KB, Moehl T. Lead iodide perovskite sensitized all-solid-state submicron thin film mesoscopic solar cell with efficiency exceeding 9%. Scientific Reports. 2012;2:591–597. DOI: 10.1038/srep00591.

[70] Noh JH, Jeon NJ, Choi YC, Nazeeruddin MK, Grätzel M, Seok S, Nanostructured TiO_2/$CH_3NH_3PbI_3$ heterojunction solar cells employing spiro-OMeTAD/Co-complex as hole-transporting material. Journal of Material Chemistry A. 2013;1:11842–11847. DOI: 10.1039/C3TA12681A.

[71] Laban WA, Etgar L. Depleted hole conductor-free lead halide iodide heterojunction solar cells. Energy and Environmental Science. 2013;6:3249–3253.DOI: 10.1039/C3EE42282H.

[72] Snaith HJ, Humphry-Baker R, Chen P, Cesar I, Zakeeruddin SM. Charge collection and pore filling in solid-state dye-sensitized solar cells. Nanotechnology. 2008;19:424003–424015. DOI: 10.1088/0957-4484/19/42/424003.

[73] Zhu K, Neale NR, Miedaner A, Frank AK. Enhanced charge-collection efficiencies and light scattering in dyesensitized solar cells using oriented TiO_2 nanotubes arrays. Nano Letters. 2007;7:69–74. DOI: 10.1021/nl062000o.

[74] Spies JA, Schafer R, Wager JF, Hersh P, PlattHAS, Keszler DA, Schneider G, Kykyneshi R, Tate J, Liu X, Compaan AJ, Shafarman WN. Pin double-heterojunction thin-film solar cell p-layer assessment. Solar Energy Materials and Solar Cells. 2009;93:1296–1308. DOI: 10.1016/J.SOLMAT.2009.01.024.

[75] Crossland JW, Noel N, Sivaram V, Leijtens T, Alexander-Webber JA, Snaith HJ. Mesoporous TiO_2 single crystals delivering enhanced mobility and optoelectronic device performance. Nature. 2013;495:215–220. DOI: 10.1038/nature11691.

[76] Tanaka K, Takahashi T, Ban T, Kondo T, Uchida K. Extremely large binding energy of biexcitons in an organic–inorganic quantum-well material $(C_4H_9NH_3)_2PbBr_4$. Solid State Communications. 2003;127:619–623. DOI: 10.1016/S0038-1098(03)00566-0.

[77] Silvia C, Edoardo M, Paolo F, Andrea L, Francesco G. $MAPbI_{3-x}Cl_x$ mixed halide perovskite for hybrid solar cells: the role of chloride as dopant on the transport and structural properties. Chemistry of Materials. 2013;25:4613–4618. DOI: 10.1016/S0038-1098(03)00566-0.

[78] Chen Q, Zhou HP, Hong ZR, Luo S, Duan HS. Planar heterojunction perovskite solar cells via vapor-assisted solution process. Journal of American Chemical Society. 2014;136:622–625. DOI: 10.1021/ja411509g.

[79] Abate A, Hollman DJ, Teuscher J, Pathak S, Avolio R. Protic ionic liquids as p-dopant for organic hole transporting materials and their application in high efficiency hybrid solar cells. Journal of American Chemical Society. 2013;135:13538–13548. DOI: 10.1021/ja406230f.

[80] Joong Jeon N, Lee J, Noh JH, Nazeeruddin MK, Grätzel M. Efficient inorganic–organic hybrid perovskite solar cells based on pyrenearylamine derivatives as hole-transporting materials. Journal of American Chemical Society. 2013;135:19087–19090. DOI: 10.1021/ja410659k.

[81] Langevin P. Recombination in low mobility semiconductors: Langevin theory. 1903; 28:433–530. DOI: 10.1038/srep08525.

[82] Christians JA, Fung RCM, Kamat PV. An inorganic hole conductor for organo-lead halide perovskite solar cells. Improved hole conductivity with copper iodide. Journal of American Chemical Society. 2014;136:758–764. DOI: 10.1021/ja411014k.

[83] Chang YH, Park CH, Matsuishi K. First-principles study of the structural and the electronic properties of the lead-halide-based inorganic-organic perovskites $(CH_3NH_3)PbX_3$ and $CsPbX_3$ (X = Cl, Br, I). Journal of Korean Physical Society. 2004;44:889–893. DOI: 10.1117/12.2054188.

[84] Yin WJ, Shi T, Yan Y. Unusual defect physics in $CH_3NH_3PbI_3$ perovskite solar cell absorber. Applied Physics Letters. 2014;104:063903–063907. DOI: 10.1063/1.4864778.

[85] Miller J. A battery material charges via an unexpected mechanism. Physics Today. 2014;67:13–15. DOI: 10.1063/PT.3.2368.

[86] Ringwood AE. The principles governing trace element distribution during magmatic crystallization 0.1. The Influence of Electronegativity. Geochimica et Cosmochimica Acta. 1955;7:189–202. DOI: 10.1016/0016-7037(56)90016-3.

[87] Wei SH, Zunger A. Electronic and structural anomalies in lead chalcogenides. Physical Review B. 1997;55:13605–13610. DOI: 10.1103/PhysRevB.55.13605.

[88] Yu LP, Kokenyesi RS, Keszler DA, Zunger A. Inverse design of high absorption thin film photovoltaic materials. Advanced Energy Materials. 2013;3:43–48. DOI:10.1002/aenm.201200538.

[89] Shockley W, Queisser HJ. Detailed balance limit of efficiency of pin junction solar cells. Journal of Applied Physics. 1961;32:510–519. DOI: 10.1063/1.1736034.

[90] Grinberg I, West DV, Torres M, Gou GY, Stein DM, Wu LY, Chen GN, Gallo EM, Akbashev AR, Davies PK, Spanier JE, Rappe AM. Perovskite oxides for visible-light-absorbing ferroelectric and photovoltaic materials. Nature. 2013;503:509–512. DOI: 10.1038/nature12622.

[91] Jarvist KTB, Frost M, Brivio F, Hendon CH, Van Schilfgaarde M, Walsh A. Atomistic origins of high-performance in hybrid halide perovskite solar cells. Nano Letters. 2014;14:2584–2590. DOI: 10.1021/nl500390f.

[92] Abrusci A, Stranks SD, Docampo P, Yip HL, Jen AKY. High performance perovskite-polymer hybrid solar cells via electronic coupling with fullerene monolayers. Nano Letters. 2013;13:3124–3128. DOI: 10.1021/nl401044q.

[93] Shi JJ, Dong J, Lv ST, Xu YZ, Zhu LF, Xiao JY, Xu X, Wu HJ, Li DM, Luo YH, Meng QB. Hole-conductor-free perovskite organic lead iodide heterojunction thin-film solar cells: high efficiency and junction property. Applied Physics Letters. 2014;104:063901–063904. DOI: 10.1039/c4cc04908j.

[94] Pellet N, Gao P, Gregori G, Yang TY, Nazeeruddin MK, Maier J, Grätzel M, Mixed-organic-cation perovskite photovoltaics for enhanced solar-light harvesting. Angewandte Chemie International Edition. 2014;53:3151–3157. DOI: 10.1002/anie.201309361.

[95] Ogomi Y, Morita A, Tsukamoto S, Saitho T, Fujikawa N, Shen Q, Toyoda T, Yoshino K, Pandey SS, Ma TL, Hayase S. $CH_3NH_3Sn_xPb_{(1-x)}I_3$ perovskite solar cells covering up to 1060 nm. Journal of Physical Chemistry Letters. 2014;5:1004–1011. DOI: 10.1021/jz5002117.

[96] Hao F, Stoumpos CC, Chang RPH, Kanatzidis MG. Anomalous band gap behavior in mixed Sn and Pb perovskites enables broadening of absorption spectrum in solar cells. Journal of American Chemical Society. 2014;136:8094–8099. DOI: 10.1021/ja5033259.

[97] Colella S, Mosconi E, Fedeli P, Listorti A, Gazza F, Orlandi TF, Besagni T, Rizzo A, Calestani G, Gigli G, De Angelis F, Mosca R. Band alignment of the hybrid halide perovskites $CH_3NH_3PbCl_3$, $CH_3NH_3PbBr_3$, $CH_3NH_3PbI_3$. Chemistry of Materials. 2013;25:4613–4618. DOI: 10.1021/cm402919x.

[98] Kulkarni SA, Baikie T, Boix PP, Yantara N, Mathews N, Mhaisalkar S. Band-gap tuning of lead halide perovskites using a sequential deposition process. Journal of Material Chemistry A. 2014:2:9221–9225. DOI: 10.1039/C4TA00435C.

[99] Sanchez RS, Gonzalez-Pedro V, Lee JW, Park NG, Kang YS, Mora-Sero I, Bisquert J. Slow dynamic processes in lead halide perovskite solar cells. characteristic times and hysteresis. Journal of Physical Chemistry Letters. 2014;5:2357–2363. DOI: 10.1021/jz5011187.

[100] Snaith HJ, Abate A, Ball JM, Eperon GE, Leijtens T, Noel NK, Stranks SD, Wang JTW. Anomalous hysteresis in perovskite solar cells. Journal of Physical Chemistry Letters. 2014;5:1511–1515. DOI: 10.1021/jz500113x.

[101] Calistru DM, Mihut L, Lefrant S, Baltog I. Identification of the symmetry of phonon modes in $CsPbCl_3$ in phase IV by Raman and resonance-Raman scattering. Journal of Applied Physics. 1997;82:5391–5395. DOI: 10.1063/1.366307.

[102] Kim J, Lee SH, Lee JH, Hong KH. The role of intrinsic defects in methylammonium lead iodide perovskite. Journal of Physical Chemistry Letters. 2014;5:1312–1317. DOI: 10.1039/c4cp04479g.

[103] Agiorgousis ML, Sun YY, ZengH, Zhang S. Electron-hole diffusion lengths exceeding 1 micrometer in an organometal trihalide perovskite absorber. Journal of American Chemical Society. 2014;136:14570–14575. DOI: 10.1021/ja5079305.

[104] Brittman S, Adhyaksa GWP, Garnett EC. The expanding world of hybrid perovskites: materials properties and emerging applications. MRS Communications. 2015;5:7–26. DOI: 10.1557/mrc.2015.6.

[105] Choi JJ, Yang XH, Norman ZM, Billinge SJL, Owen JS. structure of methylammonium lead iodide within mesoporous titanium dioxide: active material in high-performance perovskite solar cells. Nano Letters. 2013;14:127–133.DOI: 10.1021/nl403514x.

[106] Chen Q, Marco ND, Yang YM, Song TB, Chen CC, Zhao HX, Hong Z, Zhou H, Yang Y. Under the spotlight: the organic—inorganic hybrid halide perovskite for optoelectronic applications. Nano Today. 2015;10:355–396. DOI:10.1016/j.nantod.2015.04.009.

[107] Wang Q, Shao Y, Xie H, Lyu L, Liu X, Gao Y, Huang J, Qualifying composition dependent p and n self-doping in CH3NH3PbI3. Applied Physics Letters. 2014;105:163508–163513. DOI: 10.1063/1.4899051.

[108] Venkateshvaran D, et al. Approaching disorder-free transport in high-mobility conjugated polymers. Nature. 2014;515:384–388. DOI: 10.1038/nature13854.

[109] You J, Dou L, Hong Z, Li G, Yang Y. Recent trends in polymer tandem solar cells research. Progress in Polymer Science. 2013;38:1909–1928. DOI:10.1002/advs.201600032.

[110] Long Q, Dinca SA, Schiff EA, Yu M, Theil J. Electron and hole drift mobility measurements on thin film CdTe solar cells. Applied Physics Letters. 2014;105:042106–042111. DOI: 10.1063/1.4891846.

[111] Shin B, Gunawan O, Zhu Y, Bojarczuk NA, Chey SJ, Guha S. Thin film solar cell with 8.4% power conversion efficiency using an earth-abundant Cu_2ZnSnS_4 absorber. Progress in Photovoltaics: Research and Applications. 2013;21:72–76. DOI: 10.1002/pip.1174.

[112] Brown G, Faifer V, Pudov A, Anikeev S, Bykov E, Contreras M, Wu J. Determination of the minority carrier diffusion length in compositionally graded $Cu(In,Ga)Se_2$ solar cells using electron beam induced current. Applied Physics Letters. 2010;96:022104–022107. DOI: 10.1063/1.3291046.

[113] Leijtens T, Stranks SD, Eperon GE, Lindblad R, Johansson EMJ, Ball JM, Lee MM, Snaith HJ, McPherson IJ. Electronic properties of meso-superstructured and planar organometal

halide perovskite films: charge trapping, photodoping, and carrier mobility. ACS Nano. 2014;8:7147–7155. DOI: 10.1021/nn502115k.

[114] Xiao Z, Dong Q, Bi C, Shao Y, Yuan Y, Huang J. Solvent annealing of perovskite-induced crystal growth for photovoltaic-device efficiency enhancement. Advance Materials. 2014;26:6503–6509. DOI: 10.1002/adma.201401685.

[115] Dualeh A, Moehl T, Tétreault N, Teuscher J, Gao P, Nazeeruddin MK, Grätzel M. Impedance spectroscopic analysis of lead iodide perovskite-sensitized solid-state solar cells. ACS Nano. 2014;8:362–373. DOI: 10.1021/nn404323g.

[116] Gonzalez-Pedro V, Juarez-Perez EJ, Arsyad WS, Barea EM, Fabregat-santiago F, Mora-Sero I, Bisquert J. General working principles of $CH_3NH_3PbX_3$ perovskite solar cells. Nano Letters. 2014;14:888–893. DOI: 10.1021/nl404252e.

[117] Edri E, Kirmayer S, Mukhopadhyay S, Gartsman K, Hodes G, Cahen D. Elucidating the charge carrier separation and working mechanism of $CH_3NH_3PbI_{(3-x)}Cl_{(x)}$ perovskite solar cells. Nature Communications. 2014;5:3461–3471. DOI: 10.1038/ncomms4461.

[118] Tarricone L, Romeo N, Sberveglier G, Mora S. Electron and hole diffusion length investigation in CdTe thin films by SPV method. Solar Energy Materials and Solar Cells. 1982;7:343–347. DOI:10.1166/jnn.2014.8029.

[119] Mikhnenko OV, Azimi H, Scharber M, Morana M, Blom PWM, Loi MA. Exciton diffusion length in narrow bandgap polymers. Energy and Environmental Science. 2012;5:6960–6965.DOI: 10.1039/C2EE03466B.

[120] Koleilat GL, Levina L, Shukla H, Myrskog SH, Hinds S, Pattantyus-abraham AG, Sargent EH. Efficient, stable infrared photovoltaics based on solution-cast colloidal quantum dots. ACS Nano. 2008;2:833–840. DOI: 10.1021/nn800093v.

[121] Sum TC, Mathews N. Advancements in perovskite solar cells: photophysics behind the photovoltaics. Energy and Environmental Science. 2014;7:2518–2534. DOI: 10.1039/C4EE00673A.

[122] Xing G, Mathews N, Lim SS, Yantara N, Liu X, Sabba D, Grätzel M, Mhaisalkar S, Sum TC. Low-temperature solution-processed wavelength-tunable perovskites for lasing. Nature Materials. 2014;13;476–480. DOI: 10.1038/nmat3911.

[123] Sutherland BR, et al. Perovskite thin films via atomic layer deposition. Advance Materials. 2014;27:53–58. DOI: 10.1002/adma.201404059.

[124] Stuckelberger M, Niesen B, Filipic M, Moon S, Yum J, Topic M, Ballif C. Complex refractive index spectra of $CH_3NH_3PbI_3$ perovskite thin films determined by spectroscopic ellipsometry and spectrophotometry. Journal of Physical Chemistry Letters. 2015;6:66–71. DOI: 10.1021/jz502471h.

[125] Grancini G, et al. The impact of the crystallization processes on the structural and optical properties of hybrid perovskite films for photovoltaics. Journal of Physical Chemistry Letters. 2014;5:3836–3842. DOI: 10.1021/jz501877h.

[126] Even J, Pedesseau L, Jancu JM, Katan C. Importance of spin–orbit coupling in hybrid organic/inorganic perovskites for photovoltaic applications. Journal of Physical Chemistry Letters. 2013;4:2999–3005. DOI: 10.1021/jz401532q.

[127] D'Innocenzo V, et al. Excitons versus free charges in organo-lead trihalide perovskites. Nature Communications. 2014;5:3586–3590. DOI: 10.1038/ncomms4586.

[128] Huang L, Lambrecht WRL. Electronic band structure, phonons, and exciton binding energies of halide perovskites $CsSnCl_3$, $CsSnBr_3$ and $CsSnI_3$. Physical Review B. 2013;88:165203. DOI: 10.1103/PhysRevB.88.165105.

[129] Lin Q, Armin A, Nagiri RCR, Burn PL, Meredith P. Electro-optics of perovskite solar cells. Nature Photonics. 2014;9:106–112. DOI: 10.1038/nphoton.2015.

[130] Brivio F, Butler KT, Walsh A, Schilfgaarde MV. Relativistic quasiparticle self-consistent electronic structure of hybrid halide perovskite photovoltaic absorbers. Physical Review B. 2014;89:155204–155210.DOI: 10.1103/PhysRevB.89.155204.

[131] Kim HG, Becker OS, Jang JS, Ji SM, Borse PH, Lee JSA. Generic method of visible light sensitization for perovskite-related layered oxides: substitution effect of lead. Journal of Solid State Chemistry. 2006;179:1214–1218. DOI: 10.1016/j.jssc.2006.01.024.

[132] Docampo P, et al. Solution deposition-conversion for planar heterojunction mixed halide perovskite solar cells. Advance Energy Materials. 2014;4:1400355–1400362. DOI: 10.1002/aenm.201400355.

[133] Noel NK, Abate A, Stranks SD, Parrott ES, Burlakov VM, Goriely A, Snaith HJ, Al NET. Enhanced photoluminescence and solar cell performance via Lewis base passivation of organic-inorganic lead halide perovskites. ACS Nano. 2014;8:9815–9821. DOI: 10.1021/nn5036476.

[134] Wehrenfennig C, Liu M, Snaith HJ, Johnston MB, Herz LM. Homogeneous emission line broadening in the organo lead halide perovskite $CH_3NH_3PbI_3$. Journal of Physical Chemistry Letters. 2014;5:1300–1306. DOI: 10.1021/jz500434p.

[135] Maalej A, Abid Y, Kallel A, Daoud A, Lautié A, Romain F. Phase transitions and crystal dynamics in the cubic perovskite $CH_3NH_3PbCl_3$. Solid State Communications. 1997;103:279–284. DOI: 10.1039/c4ee01358a.

[136] Brittman S, Pratama Adhyaksa GW, and Garnett EC, The expanding world of hybrid perovskites: materials properties and emerging applications. MRS Communications. 2015; 5: 7-26.DOI: http://dx.doi.org/10.1557/mrc.2015.6.

[137] Umari P, Mosconi E, De Angelis F. Relativistic GW calculations on $CH_3NH_3PbI_3$ and $CH_3NH_3SnI_3$ perovskites for solar cell applications. Scientific Reports. 2014;4:4467–4470.DOI: 10.1038/srep04467.

[138] Jesper Jacobsson T, Pazoki M, Hagfeldt A, Edvinsson T. Goldschmidt's rules and strontium replacement in lead halogen perovskite solar cells: theory and preliminary experiments on $CH_3NH_3SrI_3$. Journal of Physical Chemistry C. 2015;119:25673–25683. DOI: 10.1021/acs.jpcc.5b06436.